Renewable Energy 232 (2024) 120979

Contents lists available at ScienceDirect

Renewable Energy

journal homepage: www.elsevier.com/locate/renene

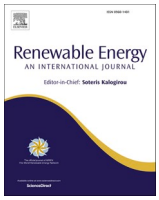

A multi-objective planning tool for the optimal supply of green hydrogen for an industrial port area decarbonization

Davide Pivetta [a,*], Alessio Tafone [b], Stefano Mazzoni [c], Alessandro Romagnoli [d], Rodolfo Taccani [a]

[a] University of Trieste, Trieste, Italy
[b] Technical University of Munich at the Singapore Campus for Research Excellence and Technological Enterprise (TUM-CREATE), Singapore, Singapore
[c] University of Roma Tor Vergata, Rome, Italy
[d] Nanyang Technological University, Singapore, Singapore

ARTICLE INFO

Keywords:
Real industrial port area
Import of hydrogen carriers
Design and operation optimization
Port decarbonization
Water electrolysis
Port hydrogen hub

ABSTRACT

This study addresses the challenge of decarbonizing highly energy-intensive Industrial Port Areas (IPA), focusing on emissions from various sources like ship traffic, warehouses, buildings, cargo handling equipment and hard-to-abate industry, typically hosted in port areas. The analysis and proposal of technological solutions and their optimal integration in the context of IPA is a topic of growing scientific interest with considerable social and economic implications. Representing the main novelties of the work, this study introduces (i) the development of a novel IPA energy and green hydrogen hub located in a tropical region (Singapore); (ii) a multi-objective optimization approach to analyse, synthesize and optimize the design and operation of the hydrogen and energy hub, with the aim of supporting decision-making for decarbonization investments. A sensitivity analysis identifies key parameters affecting optimization results, indicating that for large hydrogen demands, imported ammonia economically outperforms other green hydrogen carriers. Conversely, local hydrogen production via electrolysis becomes economically viable when the capital cost of alkaline electrolyser drops by at least 30 %. Carbon tax influences the choice of green hydrogen, but its price variation mainly impacts system operation rather than design. Fuel cells and batteries are not considered economically feasible solutions in any scenario.

Nomenclature:

Subscripts	
El	Electric
Th	Thermal
$CO_{2,eq}$	Carbon dioxide equivalent
H_2	Hydrogen
NG	Natural gas
Oil	Diesel oil
P	Photovoltaic peak power
Acronyms/Abbreviations	
ABC	Absorption Chiller
AEL	Alkaline Electrolyzer
BoP	Balance of Plant
CAPEX	CAPital EXpenditure
CC	Current Case
CCGT	Combined Cycle Gas Turbine
$CO_{2,eq}$	Carbon dioxide equivalent
EU	European Union
FC	Fuel Cells
GH_2	Gaseous hydrogen
GHG	Greenhouse Gas
HP	High Pressure
HRS	Hydrogen Refuelling Station
IEA	International Energy Agency
IPA	Industrial Port Area
LH_2	Liquid hydrogen
LOHC	Liquid Organic Hydrogen Carriers
LP	Low Pressure
MILP	Mixed Integer Linear Programming
MINLP	Mixed Integer Non-Linear Programming
NAHV	North Adriatic Hydrogen Valley
NH_3	Ammonia
O&M	Operation and Maintenance
HT-PEMFC	High-Temperature Proton Exchange Membrane Fuel Cells
PV	PhotoVoltaic
VCC	Vapour Compression Chiller

(*continued on next column*)

(*continued*)

* Corresponding author.
E-mail address: davide.pivetta@phd.units.it (D. Pivetta).

https://doi.org/10.1016/j.renene.2024.120979
Received 13 February 2024; Received in revised form 7 June 2024; Accepted 14 July 2024
Available online 25 July 2024

1. Introduction

The urge to curb pollutant and greenhouse gases (GHG) emissions under the levels set by international regulations and initiatives poses tough challenges to the entire industry, residential, transportation, and energy sectors [1], and demands for cross-sectorial approaches to ensure the effectiveness of the energy transition in the medium-long term. To this extent, a pivotal role in the energy transition may be played by the shipping and port industries, representing essential components of global trade and the economy, and handling approximately 80 % of worldwide commerce in terms of volume and 70 % in terms of value [2]. Ship traffic is the primary source of gaseous emissions, accounting for over 70 % of total emissions, while the remainder is generated by port equipment, buildings, and other industrial sectors linked to port-related activities [3].

Industrial Port Areas (IPAs) [3] encompass ports and related industries, with ports historically serving as trade facilitators and suppliers of energy and materials [4]. Being at the intersection of land and sea, IPAs are not only the backbone of the entire supply chain, but are also at the centre of vast industrial hubs that take advantage of their strategic location [5]. Consequently, IPAs are responsible for large amounts of pollutant and GHG emissions, mainly classifiable as: (i) direct emissions from cargo handling equipment and IPAs operations, (ii) indirect emissions from electric users in IPAs, and (iii) indirect emissions from industrial plants located in IPAs [6]. Moreover, since more than 90 % of ports are located in proximity of metropolitan and city areas, IPAs have a significant environmental impact on neighbouring areas, posing serious health risks [7].

For this reason, the last years have seen a growing interest in the definition of decarbonization pathways for IPAs, as demonstrated also by several European Union (EU) initiatives [8,9]. Indeed, IPAs could act as facilitators of the decarbonization of multiple sectors, from the maritime transportation to the hard-to-abate industries [5], enabling the establishment of green energy hubs and clean fuels infrastructures [10].

However, the IPAs decarbonization is a complex issue that involves several stages of the production chain. The IPAs decarbonization strategies can be mainly categorized as energy efficiency initiatives, logistic planning/optimization, and use of renewable energy sources (RES) [11,12]. The latter could directly supply clean electricity to the electrified cargo handling and logistic fleet vehicles, to industrial plants located in the IPAs (e.g. steel plants electric arc furnaces), or to ships at berth (i.e. cold ironing) [13]. Zhang et al. [14] emphasised that the success of port decarbonization lies in the evaluation of RES and alternative fuels that are best suited to the characteristics of single ports. Karagkouni et al. [15] pointed out that the most explored solutions for port decarbonization include (i) onshore energy supply, (ii) alternative fuels, (iii) circular economy and (iv) waste management. Iris et al. [11] carried out a systematic analysis of operational techniques, technologies, and energy management systems that can help decrease GHG emissions and improve energy efficiency in port areas. From the literature review, the use of RES emerges as one of the most promising strategies for reducing the $CO_{2,eq}$ emission of IPAs, with solar energy being the most widely used form of RES in ports. High-capacity photovoltaic (PV) plants in IPAs are commonly installed on building rooftops [16]. Another effective strategy to reduce the carbon footprint of IPAs is the implementation of smart grids that combine RES power plants with energy storage technologies. In this context, Ahamad et al. [17] investigated the potential benefits of using RES-based smart grids in IPAs.

Pivetta et al. [18] proposed a comprehensive review of decarbonization strategies for IPAs, with a particular focus on the role that green hydrogen (H_2) could play when used as renewable energy carrier. In fact, H_2 produced from RES could be used for the production of green fuels (e.g. ammonia, H_2) used in IPAs to power the cargo handling equipment [19] and ships [20,21], be utilized in stationary fuel cells (FC) to meet the electricity needs of ports [22] or substitute carbon intensive chemical feedstocks in industrial plants [23]. The use of RES to produce green fuels, and particularly H_2, has seen a growing interest in the last years, and several IPAs have recently outlined strategies for becoming not only energy hubs, but also H_2 hubs [5,24]. Indeed, several ongoing projects aim to develop H_2 infrastructures for port and industrial use, such as in the Port of Valencia and the Port of Rotterdam [23,25]. This is the concept of the regional, large-scale and industry-focused H_2 valleys, i.e. “regional ecosystems that link H_2 production, transportation, and various end uses such as mobility or industrial feedstock” [26]. In this framework, green H_2 can indeed play a key role for coupling different industrial and economic sectors, such as maritime, oil and gas, cruise-based-tourism, bulk distribution and transformation, thermal power plants, electricity grid operators and offshore wind, which are typically hosted in port areas [5]. The main bottlenecks of this strategy are represented by the high costs of large-scale electrolyzers, lack of standards in IPAs, and limited surface availability for RES installation, particularly where offshore power plants are not feasible (e.g., offshore wind turbines) [11,18]. Importing green H_2 is also another viable alternative to reduce the use of fossil fuels and mitigate carbon impact [24]. Ammonia (NH_3) is also a promising solution as a direct or indirect H_2 carrier, and its share in the maritime sector’s fuel mix could increase from 7 % in 2030 to 20–25 % in 2050 [27].

One of the major international maritime transport hubs is represented by the city-state Singapore, a country characterized by a typical tropical climate. Indeed, the Port of Singapore is currently the world’s second busiest port in terms of container throughput, with ship arrival tonnage exceeding 2.8 billion gross tonnes in 2021 [28]. Within its energy strategy toward 2050 [29], Singapore aims to halve emissions from its peak to $33Mt_{CO2eq}$ by 2050, potentially achieving net-zero emissions with the adoption different strategies to decarbonize the grid while guaranteeing energy security and affordability. In this context, first in 2011 with the Maritime Singapore Green Initiative programme [30] and recently through the “Maritime Singapore Decarbonization blueprint” [28], Singapore has promoted the adoption of the following sustainability practices within the port and shipping sectors: 1) the use of green electricity either locally produced in port area or imported from regional grid; 2) the use of alternative marine fuels (i.e. H_2, NH_3, etc.) for both cargo handling equipment and tugboats; 3) the replacement of diesel-powered cranes with electric-automated systems and 4) the introduction of energy efficiency measures for buildings and warehouses.

All those strategies for IPAs decarbonization are not concurrent, but more likely complementary for achieving the decarbonization goals and, most importantly, to maintain the goals in the medium-long term, as also explained in Ref. [31].

However, the choice of the best combination of initiatives involves a large set of decision variables and must account for the uncertainty that intrinsically affects the RES availability. To this extent, energy modelling and optimization can give a substantial support to the decision-making process for both local stakeholder and policymakers. Starting from the definition of the IPAs demands (i.e., electricity, cooling, heating, H_2, etc.), energy models allow to determine the optimal combination of energy conversion and storage units (synthesis), their sizes (design) and their operating conditions (operation) that guarantee the achievement of the desired objective function, e.g. either in terms of cost or emission reductions.

Although, as previously shown, port decarbonization is a topic of great interest in the fields of energy and environmental engineering, there is a lack of comprehensive studies that analyse and synthesize the various energy demands (mechanical, electrical, heating, and cooling) of IPAs. Moreover, the design and optimization of alternative energy systems for ports are often overlooked at the global system level. Indeed, although previously developed tools [32,33] demonstrated how energy

models could be useful not only for the scientific community, but also for the industrial and commercial ones, it appears to be a lack of tools that simultaneously optimize an IPAs as a whole, taking into account energy and fuel needs of different IPAs users and combining different decarbonization strategies.

In this context, the present work aims to overcome these research gaps in the literature and goes a step further, introducing the following novelties representing the real driving force of the paper: 1) the development of a novel IPA energy and green-H_2 hub located in Singapore; 2) a general synthesis, design, and operation optimization tool able to define the best combination of decarbonization strategies to achieve environmental and economic benefits of the IPA under different energy and market scenarios.

Considering the environmental targets set by the Port of Singapore, this study proposes the estimation of typical energy and H_2 demands and associated carbon dioxide equivalent ($CO_{2,eq}$) emissions of: port warehouses and buildings, tugboats, yard tractors and cranes operating in port, and a Combined Cycle Gas Turbine (CCGT) power plant. The energy and H_2 demands are representative of the typical energy needs of a large Asian port located in a tropical area and a potential H_2 demand of co-located power plants or heavy industries (i.e. steel, chemical and refining industries), whose decarbonization process may require green H_2 in the future. A set of different energy solutions and energy system configurations has been proposed to meet the IPA energy demand at a reduced $CO_{2,eq}$ emissions. In particular, the exploitation of local RES, electric and thermal energy storage systems, and technologies for H_2 import/production, storage and utilization have been investigated. Furthermore, the model comprises also technologies to convert Liquid Organic H_2 Carriers (LOHC), NH_3 and Liquefied H_2 (LH_2) into H_2 to be used in power plant and for hybrid H_2 vehicles. A multi-objective approach has been adopted through a Mixed-Integer Linear Programming (MILP) algorithm to concurrently optimize techno-economic and environmental objective functions and to describe energy conversion and storage units, tackling complex optimization problems while avoiding excessive computational effort. Given the uncertainty in the value of some of the tool's input variables, in particular the costs of H_2carriers and technologies such as electrolysers and fuel cells, a sensitivity analysis was carried out to investigate the extent to which these parameters influence the optimal choice of energy system design and operation variables.

In the following, Section 2 presents the modelling and optimization approach here proposed by the authors, while Section 3 describes the energy system of the analysed IPA, introducing the energy demands and the proposed different energy system configurations. Section 4 presents and discusses the main results of the optimizations. Section 5 outlines the conclusions.

2. Modelling and optimization approach

This section introduces the general methodology adopted to model and optimize the energy system configurations proposed for the IPA decarbonization. Models of energy conversion and storage units proposed to be installed in IPA are also presented. The general features of the optimization problem are first outlined, with specific emphasis on the choice of the different objective functions and on the characteristics of the equations included in the model of each energy conversion and storage units. The energy models were developed from a previous work carried out by the authors [34] who developed a preliminary calculation tool to optimally select the set of decarbonization strategies for the IPA of Trieste (Italy), taken as a case study.

Mixed Integer Non-Linear Programming (MINLP) is a commonly utilized technique in energy systems optimization problems, providing a comprehensive representation of the functioning of individual energy conversion and storage units within the system. Nevertheless, when applied to large-scale energy systems composed of numerous interconnected energy units, the computational cost of MINLP methods become substantial due to the significant number of real and integer decision variables required for system design and operation [35,36]. To tackle this challenge, several researchers [37,38] suggest a simplification of MINLP into a Mixed Integer Linear Programming (MILP) approach. In this approach, both the non-linear characteristics and constraints associated with the energy units can be approximated as linear without significant loss of accuracy [36,39–41], especially when dealing with highly integrated energy systems. Accordingly, the computational cost required for solving the constrained optimized problem of the design and operation optimization of the energy system is significantly reduced. Given the complexity related to the high level of integration of the energy systems depicted in Fig. 2 and the dynamic nature of the optimization problem, this study opts for the utilization of a MILP approach.

The general MILP optimization problem is formulated as in Eq. (1) [42]:

$$\underbrace{\min}_{x,y} \left(\boldsymbol{c}^T\boldsymbol{x} + \boldsymbol{d}^T\boldsymbol{y}\right) \quad s.t.\ \boldsymbol{A}\boldsymbol{x} + \boldsymbol{B}\boldsymbol{y} = \boldsymbol{b} \tag{1}$$

where $\boldsymbol{x} \geq \boldsymbol{0} \in \mathbb{R}^{N_x}, \boldsymbol{y} \in \{0,1\}^{N_y}$.

in which c and d are the cost arrays associated with the continuous and binary variables, x and y, respectively; A and B are the equality constraint matrices and b is the constraint known term; N_x and N_y indicate the dimension of x and y, respectively.

The design-operation optimization problem of the energy system proposed in Fig. 2 is formulated considering the following objective functions, decision variables and constraints.

- Objective functions: the total cost and the $CO_{2,eq}$ emissions are both minimized, placing a different "weight" for the two objective functions in the multi-objective optimization.
- Decision variables: continuous, integer, and binary variables associated with the design and operation of the energy system.
- Constraints: equalities and inequalities associated with the performance and operational limits of the energy conversion and storage units.

The optimization problem is implemented in Python programming language [43] and solved with the optimizer Gurobi [44].

Section 2.1 presents the models of the energy conversion and storage proposed for the IPA alternative energy system configuration. Section 2.2 introduces the methodology applied for the optimization of the design and operation of the proposed energy system.

2.1. Model of energy conversion and storage units

The operation of each energy conversion unit i is modelled by its characteristic curve. In general, the characteristic curve of an energy conversion unit takes the following steady-state form [36,45,46]:

$$\phi_{in,i}(t) = k_{1i} \cdot \phi_{out,i}(t) + k_{2i} \cdot \delta_i(t) \tag{2}$$

$$\phi_{out,i}(t) \leq \phi_{MAX_{out,i}} \cdot \delta_i(t) \tag{3}$$

$$\phi_{out,i}(t) \geq \phi_{MIN_{out,i}} \cdot \delta_i(t) \tag{4}$$

Where $\phi_{in,i}(t)$ is the energy flow associated with the main input to a unit, $\phi_{out,i}(t)$ is the energy flow associated with the main output of the unit, $\phi_{MAX_{out,i}}$ and $\phi_{MIN_{out,i}}$ are the maximum and minimum loads of the unit, respectively, k_{1i} and k_{2i} are (usually positive) parameters depending on the type and features of the energy conversion unit, and $\delta_i(t)$ is a binary variable that identifies the on/off status of the unit. When $\delta_i(t) = 0$, Eqs. (3) and (4) give $\phi_{out,i}(t) = 0$ and so Eq. (2) gives $\phi_{in,i}(t) = 0$, i.e., the unit is off. When $\delta_i(t) = 1$, Eqs. (3) and (4) let $\phi_{out,i}(t)$ vary within the range

of possible loads and the fuel consumption is calculated by Eq. (2), i.e., the unit is on.

The general formulation to describe the design and operation of energy storage units is defined in the following, as proposed by Ref. [36]. Eq. (5) relates the energy stored at time t ($\varepsilon_j(t)$) with the energy stored a time t-1 ($\varepsilon_j(t-1)$) and the energy entering ($\phi_{in,j}(t)$) or outgoing from ($\phi_{out,j}(t)$) the energy storage unit. The "charge" and "discharge" efficiencies of the energy storage unit are considered ($k_{1,j}$, $k_{2,j}$). As shown in Eq. (6), the minimum and maximum of the energy that can be stored in the unit are also considered using fixed parameters ($k_{3,j}$ and $k_{4,j}$) and are related to the design variable $\varepsilon_{j_{max}}$.

$$\varepsilon_j(t) = \varepsilon_j(t-1) + k_{1,j}\cdot\phi_{in,j}(t) - k_{2,j}\cdot\phi_{out,j}(t) \tag{5}$$

$$k_{3,j}\cdot\varepsilon_{j_{max}} \le \varepsilon_j(t) \le k_{4,j}\cdot\varepsilon_{j_{max}} \tag{6}$$

Following subsections introduces the models of energy conversion and storage units proposed for the case study of the Singapore's IPA. For the j-th energy component, D_j variables define the design variables, δ_j the binary variables identifying the on/off status or the inclusion/exclusion. The continuous variables identify: the electric power flows (P_j), the H_2 flows (H_j), the cooling flows (Q_j), and the heating flow (QH_j).

Supplementary Material reports all the technical and economic characteristics of conversion and storage technologies selected in this study.

2.1.1. Photovoltaic system

Model of a generic PV system is here considered. Taking into account the installation on the roofs of warehouses and buildings, crystalline silicon PV panels are proposed for the proposed IPA. Data related to the PV production are collected by using open-source software available online [47]. In the calculation, it is assumed a 12 % PV system loss, no solar tracking system, and a tilt angle and azimuth angle equal to 0°. Data about the solar production of a generic PV panel installed in Singapore were retrieved from Ref. [47] for 1.3571 latitude and 103.8195 longitude. Power production profile in a typical week is estimated by data available over the year, considering "MERRA-2" Dataset.

Power produced by the PV (P_{PV}) is determined as the direct normal irradiance ($DNI(t)$) multiplied by a fixed efficiency of the PV (η_{PV}). PV power in the IPA has been limited to 30 MW_P based on the surface area available for installation.

$$P_{PV}(t) = D_{PV}\cdot DNI(t)\cdot\eta_{PV} \tag{7}$$

2.1.2. National electric grid

The national power grid allows the supplying/purchasing of power to/from the port internal grid. The power capacity of national power grid is supposed to be infinite both for the supplying and the purchasing. Power losses due to the power transfer to/from the port internal grid are neglected. The average price of energy bought/sold from/to the national grid during the week is assumed based on data retrieved from Ref. [48]. The carbon footprint of electricity purchased from the grid is assessed from Ref. [49]. Fixed costs associated with the capability of the electrical grid are considered. The capacity of the grid is evaluated as the highest value that represents the power withdrawn from ($P_{el,p}$) or supplied to the grid ($P_{el,n}$).

2.1.3. Low-pressure and high-pressure compressors

The study presents a simplified thermodynamic model for H_2 compression at two pressure levels. The first compression stage involves a two-stage process from 30 to 300 bar, where the H_2 is defined as Low-Pressure (LP) H_2. This H_2 can either be stored or used directly to supply the industrial H_2 demand. The second stage encompasses the compression of H_2 to 820 bar, where the H_2 is defined as High-Pressure (HP) H_2, which can be stored and used to refuel H_2 vehicles equipped with compressed H_2 tanks at 700 bar.

The compression station makes use of reciprocating compressors. The advantage of reciprocating compressors compared to centrifugal ones is three-fold: (i) allow higher pressure ratios, (ii) are more robust and have longer lifetimes and (iii) sealings are better suited to the properties of H_2 (small molecule, high diffusivity).

A general equation to calculate the power require for compressing an ideal gas is reported in Eq. (8). The electric power P_{comp} (kW) absorbed by a compressor is calculated starting from the specific work of the adiabatic isentropic compression $L_{comp,is}$ (kJ/kg) and considering constant efficiency for mechanical (η_{mech}), isentropic (η_{is}), and electric (η_{el}) processes. $\delta_{comp}(t)$ is the binary variable that defines the on/off status of the compressors.

$$P_{comp}(t) = \dot{H}(t)\cdot\frac{L_{comp,is}}{\eta_{is}\cdot\eta_{mech}\cdot\eta_{el}}\cdot\delta_{comp}(t) \tag{8}$$

Eqs. (9)–(11) describe the operation of a general compression station (LP or HP). Eq. (9) relates the power required by the compressor with the H_2 flow entering the compressor a time t, while Eq. (10) determines the heat generated during compression that could be recovered by the intercooler system. Eq. (11) limits the load variation of the compressor. The intercooler system installed between the two compression stages is also equipped with a heat dissipation unit.

$$P_{comp,j}(t) = k_{1_{comp\,j}}\cdot\dot{H}_j(t) \tag{9}$$

$$QH_{comp,j}(t) = k_{2_{comp\,j}}\cdot\dot{H}_j(t) \tag{10}$$

$$k_{MIN_{comp_j}}\cdot D_{comp_j} \le P_{comp,j}(t) \le k_{MAX_{comp_j}}\cdot D_{comp_j} \tag{11}$$

2.1.4. Alkaline electrolyzer

The local production of H_2 via electrolysis is considered. Alkaline Electrolyzer (AEL) technology is considered in this study as it is commonly preferred for localized H_2 production in industrial sector due to their various advantages over Solid Oxide Electrolyzer (SOE) and Proton Exchange Membrane Electrolyzer (PEME). SOE have the potential to be a good option for H_2 production in industrial plants due to their high temperature operation and efficiency. However, their low technological maturity and high material costs currently limit their large-scale use. PEME have a higher efficiency and are more flexible in operation compared to AEL. However, when the AEL is coupled to a battery and/or connected to the grid, as in the case study proposed by the authors, the start-up time and the time required for load variation do not affect the operation of the AEL if it can be kept running when solar power is temporarily unavailable. If the electrolyser is switched off for a few hours, the time required for a "warm" start-up of the AEL is only slightly longer than that required by a PEME. Given the recent performance improvements of electrolysers provided by some suppliers (e.g. by De Nora [50]), AEL are often proposed in energy systems coupled with RES plants [51]. The advantages of AEL over PEME are also the higher operating temperatures that facilitate the waste heat recovery and the lower investment and maintenance costs.

Following equations describe the design and operation of the AEL. Eq. (12) defines the hourly mass flow rate ($\dot{H}_{LP,elect}(t)$, kg/h) of H_2 produced at 30 bar by the AEL is defined as function of the power absorbed by the AEL ($P_{elect}(t)$, kW), and a proportionality coefficient ($k_{1,elect}$), which is determined according to the linearization of the performance curve of a typical AEL at different power load. $\delta_{elect}(t)$ is the binary variable accounting for the on/off status of the AEL. Heat power generated during AEL operation ($QH_{elect}(t)$, kW_{th}) can be recovered, as expressed in Eq. (13). When heat is not recovered and used, a heat dissipation unit is considered. The absorbed electric power is constrained in Eq. (14) not to exceed the power load range. The power bounds are expressed as percentages $k_{MIN_{elect}}$ and $k_{MAX_{elect}}$ of the AEL nominal power D_{elect} (kW).

$$\dot{H}_{LP,elect}(t) = \left(k_{1,elect} \cdot P_{elect}(t) + k_{2,elect} \cdot D_{elect}\right) \cdot \delta_{elect}(t) \quad (12)$$

$$QH_{\text{elect}}(t) = k_{3_{elect}} \cdot P_{elect}(t) \cdot \delta_{elect}(t) \quad (13)$$

$$k_{MIN_{elect}} \cdot D_{elect} \leq P_{elect}(t) \leq k_{MAX_{elect}} \cdot D_{elect} \quad (14)$$

2.1.5. Stationary fuel cells

Performance and cost of High-Temperature Proton-Exchange Membrane FC (HT-PEMFC) for stationary application are considered in this study. Among different FC technologies, HT-PEMFCs are chosen as a compromise between cost, technological maturity, tolerance to impurities in H_2 supplied to FC and operational flexibility [52].

Following equations (Eqs. (15)–(17)) describe the HT-PEMFC design and operation. Performance and cost parameters are retrieved from Refs. [52,53] and are reported in Supplementary Material. Eq. (15) relates the H_2 required by the HT-PEMFC with the power produced by the HT-PEMFC, while Eq. (16) evaluates the heat that could be recovered by the HT-PEMFC operation. Eq. (17) limits the load variation of the HT-PEMFC. It is assumed that the HT-PEMFC is equipped with a heat dissipation unit.

$$\dot{H}_{FC}(t) = \left(k_{1_{FC}} \cdot P_{FC}(t) + k_{2_{FC}} \cdot D_{FC}\right) \cdot \delta_{FC}(t) \quad (15)$$

$$QH_{FC}(t) \leq \left(k_{3_{FC}} \cdot P_{FC}(t) + k_{4_{FC}} \cdot D_{FC}\right) \cdot \delta_{FC}(t) \quad (16)$$

$$k_{MIN_{FC}} \cdot D_{FC} \leq P_{FC}(t) \leq k_{MAX_{FC}} \cdot D_{FC} \quad (17)$$

2.1.6. Absorption chiller

Eqs. (18) and (19) describe the design and operation of a generic Absorption Chiller (ABC). For the defined case study, an ABC was chosen, operating at a temperature of 80–120 °C and 7–12 °C for the hot and cold side respectively. Performance parameters of the ABC ($k_{1_{ABC}}, k_{2_{ABC}}, k_{MIN_{ABC}}, k_{MAX_{ABC}}$) are retrieved from Refs. [54,55] and reported in Supplementary Material.

In Eq. (18), the cooling generated by the ABC ($Q_{ABC}(t)$) is related to the heat supplied to the absorber ($QH_{ABC}(t)$). Heat entering the chiller is limited by the possible load variation of the chiller, as described in Eq. (19). The energy requirement of the ABC for its operation is relatively low compared to the heat required by the absorption process (QH_{ABC}) and is therefore considered negligible in this study.

$$Q_{ABC}(t) = \left(k_{1_{ABC}} \cdot QH_{ABC}(t) + k_{2_{ABC}} \cdot D_{ABC}\right) \cdot \delta_{ABC}(t) \quad (18)$$

$$k_{MIN_{ABC}} \cdot D_{ABC} \leq QH_{ABC}(t) \leq k_{MAX_{ABC}} \cdot D_{ABC} \quad (19)$$

2.1.7. Vapour compression chiller

Vapour Compression Chillers (VCC) fed by electricity are already installed in the considered IPA and fully match the cooling demand required by the port buildings and warehouses. Eq. (20) relates the power required by the VCC ($P_{VCC}(t)$), with the cooling energy generated ($Q_{VCC}(t)$), while Eq. (21) limits its load variation.

Due to the hot and humid climate of the sub-tropical/equatorial region [56], in the proposed model, the heating bus is not taken into consideration. Techno-economic characteristics of the VCC considered in the optimizations are reported in Supplementary Material.

$$Q_{VCC}(t) = \left(k_{1_{VCC}} \cdot P_{VCC}(t) + k_{2_{VCC}} \cdot D_{VCC}\right) \cdot \delta_{VCC}(t) \quad (20)$$

$$k_{MIN_{VCC}} \cdot D_{VCC} \leq P_{VCC}(t) \leq k_{MAX_{VCC}} \cdot D_{VCC} \quad (21)$$

2.1.8. Hydrogen refuelling stations

H_2 refuelling stations (HRS) are divided into two types: one dedicated to the refuelling ofthe yard tractors fleet and one for bunkering H_2 to the tugboats. The two different types differ only by the maximum capacity to supply H_2 to equipment and vehicles in terms of kg supplied per hour and per day, and costs. HP H_2 storage supplies H_2 to the HRS at 820 bar. This pressure is high enough such that HRS does not need an additional compressor unit to supply H_2 equipment and vehicles assuming they have an on-board H_2 tank operating at 700 bar pressure. Each HRS is equipped with a refrigerator unit, which cools down the H_2 to −40 °C, avoids the heating of the H_2 and, in turn, ensures full fillings of the on-board equipment and vehicle tanks (referring to the standard SAE-J2601 [57]). Therefore, HRS requires electric power $P_{refr}(t)$ for the refrigeration of H_2 mass flow rate ($H_{j_{OUT}}(t)$). In Eq. (22), COP is the coefficient of performance of the chiller, $h_{storage}$ and $h_{dispenser}$ are respectively the H_2 enthalpies in the HP storage and at the dispenser outlet, which are evaluated using CoolProp [58,59].

$$P_{refr}(t) = \frac{\dot{H}_{j_{HRS}}(t) \cdot \left(h_{storage} - h_{dispenser}\right)}{COP} \quad (22)$$

2.1.9. Electric storage system

Lithium-Ion Batteries (LIB) are well proven technologies to store electric energy for both industrial, residential and mobility applications. Among other types of electric storage solutions (e.g. lead-acid batteries and capacitors), LIB are chosen in this study as good compromise between costs, energy density, voltage fluctuations of the output power and modularity [60].

The integral form of the electric energy balance at the LIB is expressed in Eq. (23). Equation states that the electric energy in the storage $E_{batt}(t)$ at time t is equal to the electric energy in the storage $E_{batt}(t-\Delta t)$ at the preceding time plus the electric power entering to (P^{-}_{batt}) and minus the electric power exiting from (P^{+}_{batt}) the storage, both multiplied by the time step (Δt). η_{batt} is the charging/discharging efficiency. As described by Eq. (24), the electric energy in the storage lies between a minimum and a maximum state of charge, which are set as percentages ($k_{MIN_{batt}}$ and $k_{MAX_{batt}}$) of the battery design capacity (D_{batt}). Eq. (25) imposes that the electric energy stored at the first-time step must equal to the energy at the end of the simulation period.

$$E_{batt}(t) = E_{batt}(t-\Delta t) + \eta_{batt} \cdot P^{-}_{batt} \cdot \Delta t - (1/\eta_{batt}) \cdot P^{+}_{batt} \cdot \Delta t \quad (23)$$

$$k_{MIN_{batt}} \cdot D_{batt} \leq E_{batt}(t) \leq k_{MAX_{batt}} \cdot D_{batt} \quad (24)$$

$$E_{batt}(0) = E_{batt}(t_{end}) \quad (25)$$

2.1.10. Cold thermal energy storage

A single thermocline tank operating with water is here considered as cold Thermal Energy Storage (TES). The design and operation of the tank are described by the following equations. The thermal energy in the storage lies between a minimum and a maximum state of charge, which are set as percentages ($k_{MIN_{TES}}$ and $k_{MAX_{TES}}$) of the TES design capacity (D_{TES}), as defined in Eq. (26). Eq. (27) is the energy balance at time t, expressed as the volume of water stored in the tank. Eq. (28) imposes the tank at the beginning to be at the same level as at the end of the optimization period (t_{fin}). This guarantees that the thermal energy generated by the energy conversion units during t_{fin} is equal to the sum of the energy required by the users plus the losses of the storage units.

$$k_{\text{MIN}_{TES}} \cdot D_{TES} \leq E_{batt}(t) \leq k_{MAX_{TES}} \cdot D_{TES} \quad (26)$$

$$Q_{TES}(t) = Q_{TES}(t-\Delta t) + \left(\dot{Q}_{ABC} \cdot \Delta t + \dot{Q}_{WCC} \cdot \Delta t\right) \cdot k_{1_{TES}} - \dot{Q}_{demand} \cdot \Delta t \Big/ k_{1_{TES}} \quad (27)$$

$$Q_{TES}(0) = Q_{TES}(t_{fin}) \quad (28)$$

2.1.11. Low-pressure and high-pressure hydrogen storage

The integral form of the mass balance at the LP H_2 storage and at the HP H_2 storage are defined in Eq. (29) and Eq. (30), respectively. Equations state that the mass in the storage $H_{S_{LP}}(t)$ and $H_{S_{HP}}(t)$ (expressed in kg) at time t is equal to the mass in the storage $H_{S_{LP}}(t-\Delta t)$ and

$H_{S_{HP}}(t-\Delta t)$ (kg) at the preceding time plus/minus the mass flow rates entering to ($\dot{H}_{in_{LP}}$ and $\dot{H}_{in_{HP}}$, kg/h) or exiting from ($\dot{H}_{out_{LP}}$, $\dot{H}_{out_{HP}}$, kg/h) the storage multiplied by the time step (Δt, h). H_2 entering and leaving storage is subject to a round trip efficiency (η_{RTES}). However, these losses are considered negligible (η_{RTES} is set equal to 1) compared to the losses caused by the compressor. In addition, a pressure difference between storage and the point of H_2 use (for CCGT and vehicle tanks) is assumed in this analysis in order to consider the pressure losses due to the distribution and storage of H_2 without requiring subsequent compression.

$$H_{S_{LP}}(t) = H_{S_{LP}}(t-\Delta t) + \eta_{RTE_S}\cdot\dot{H}_{in_{LP}}\cdot\Delta t - \dot{H}_{out_{LP}}\cdot\Delta t \quad (29)$$

$$H_{S_{HP}}(t) = H_{S_{HP}}(t-\Delta t) + \eta_{RTE_S}\cdot\dot{H}_{in_{HP}}\cdot\Delta t - \dot{H}_{out_{HP}}\cdot\Delta t \quad (30)$$

For both the LP and HP H_2 storage, the mass in the storage varies between a minimum and a maximum set as percentages ($k_{\min_{HS}}$ and $k_{max_{HS}}$, %) of the storage design capacity ($D_{S_{LP}}$ and $D_{S_{HP}}$, kg) (Eqs. (31) and (32)). Moreover, the stored mass at the first-time step must equal that at the end of the simulation period, i.e. a year operation (Eqs. (33) and (34)).

$$k_{MIN_{HS}}\cdot D_{S_{LP}} \le H_{S_{LP}}(t) \le k_{MAX_{HS}}\cdot D_{S_{LP}} \quad (31)$$

$$k_{MIN_{HS}}\cdot D_{S_{HP}} \le H_{S_{HP}}(t) \le k_{MAX_{HS}}\cdot D_{S_{HP}} \quad (32)$$

$$H_{S_{LP}}(0) = H_{S_{LP}}(t_{fin}) \quad (33)$$

$$H_{S_{HP}}(0) = H_{S_{HP}}(t_{fin}) \quad (34)$$

2.1.12. Ammonia

NH_3 is one of the H_2 carriers that can be easily imported by ports via ship. When NH_3 arrives in port, it can be converted into pure H_2 required by the port vehicles and equipment, and/or the industry by using an NH_3 cracking system. NH_3 cracking is an endothermic process that requires catalysts and high temperature to allow the H_2 conversion with high efficiency and high grade of purity. The typical operation of a NH_3 cracking system for industrial use is considered in this study [61]. A minimum size of the cracker is defined in Eq. (37) and its load is limited by the $k1_{cracker}$ and $k2_{cracker}$ performance parameters in Eq. (36). Eq. (35) relates the NH_3 entering the cracker to the H_2 outgoing from the cracker, subjected to an energy efficiency expressed by the coefficient $k3_{cracker}$. Eq. (38) defines the design of the NH_3 storage system, evaluated as the sum of NH_3 required during the entire optimization period from t_{in} to t_{fin}. This assumption is considered in such a way that the NH_3 storage can satisfy the entire weekly NH_3 demand of the plant and can modulate the possible variation of NH_3 supplied by ship.

$$H_{NH_3}(t) = k3_{cracker}\cdot ship_{NH_3}(t)\cdot\delta_{cracker}(t) \quad (35)$$

$$k1_{cracker}\cdot D_{cracker}\cdot\delta_{cracker}(t) \le ship_{NH_3}(t) \le k2_{cracker}\cdot D_{cracker}\cdot\delta_{cracker}(t) \quad (36)$$

$$D_{cracker_{min}} \le D_{cracker} \quad (37)$$

$$D_{S_{NH_3}} = \sum_{t_{in}}^{t_{fin}} H_{NH_3}(t) \quad (38)$$

2.1.13. Liquefied hydrogen

LH_2 can be efficiently transported via ship also for long distances, given its higher energy density respect to the compressed H_2 and other H_2 carriers (NH_3 and LOHC). LH_2 vapour can be directly use as fuel by FC operating at low temperature (es. PEMFC) without needing purifying systems. When LH_2 arrives in port, it is vaporized in a regasification unit with a fixed efficiency ($k3_{LH2}$), as described by Eq. (39). Eq. (40) relates the cooling recovered in the regassification units with the H_2 flow rate. Data of commercially available technologies for vaporizing LH_2 are here considered to estimate costs and performance of the system [62]. Similarly to the storage of NH_3, as described in Eq. (38), Eq. (43) imposes that the size of LH_2 storage tank is equal to the H_2 demand during the entire optimization period (one week).

$$H_{LH_2}(t) = k3_{LH_2}\cdot ship_{LH_2}(t)\cdot\delta_{LH_2}(t) \quad (39)$$

$$Q_{LH_2}(t) = k4_{LH_2}\cdot ship_{LH_2}(t)\cdot\delta_{LH_2}(t) \quad (40)$$

$$k1_{LH_2}\cdot D_{LH_2}\cdot\delta_{LH_2}(t) \le ship_{LH_2}(t) \le k2_{LH_2}\cdot D_{LH_2}\cdot\delta_{LH_2}(t) \quad (41)$$

$$D_{LH_{2min}} \le D_{LH_2} \quad (42)$$

$$D_{S_{LH_2}} = \sum_{t_{in}}^{t_{fin}} H_{LH_2}(t) \quad (43)$$

2.1.14. Liquid Organic hydrogen carrier

When LOHC arrives in the port, a dehydrogenation system is considered to convert LOHC into pure H_2. Three types of LOHC are considered in the analysis, namely Dibenzyltoluene, N-Ethyl-Carbazole, and Toluene. Typical performance and costs of commercial technologies used in dehydrogenation units are considered [63,64]. Eq. (44) relates the LOHC entering the dehydrogenation units to the H_2 outgoing from dehydrogenation units, subjected to an energy efficiency expressed by $k3_{LOHC}$. Power demand required by the dehydrogenation unit is expressed as function of the LOHC entering the dehydrogenation unit (Eq. (45)). Eqs. (46) and (47) limits the load variation and the minimum size of the dehydrogenation unit, respectively. The size of LOHC storage system is evaluated to store the amount of LOHC required for the entire optimization period (Eq. (48)), as defined for the other H_2 carriers.

$$H_{LOHC}(t) = k3_{LOHC}\cdot ship_{LOHC}(t)\cdot\delta_{LOHC}(t) \quad (44)$$

$$P_{LOHC}(t) = k4_{LOHC}\cdot ship_{LOHC}(t)\cdot\delta_{LOHC}(t) \quad (45)$$

$$k1_{LOHC}\cdot D_{LOHC}\cdot\delta_{LOHC}(t) \le ship_{LOHC}(t) \le k2_{LOHC}\cdot D_{LOHC}\cdot\delta_{LOHC}(t) \quad (46)$$

$$D_{LOHC_{min}} \le D_{LOHC} \quad (47)$$

$$D_{S_{LOHC}} = \sum_{t_{in}}^{t_{fin}} H_{LOHC}(t) \quad (48)$$

2.2. Objective functions

The MILP models are optimized by using Gurobi solver [44]. A "Blended Objectives" method was adopted, considering a linear combination of the objective functions, each with a fixed weight [65]. A 1 % deviation from the optimal value of the combined objective function has generally been allowed by means of the "MIPgap" command in Gurobi [44]. In the following, the general formulation of the cost objective function and the emission (in term of $CO_{2,eq}$ emission) objective function are presented.

$$f_{cost} = \sum D_j\cdot\left(C_{inv,a_j} + C_{rep,a_j} + C_{O\&Mj}\right) + \sum c_j\cdot\left(P_j + H_j + F_j\right) \quad (49)$$

$$f_{CO_2} = \sum c_{CO2_j}\cdot\left(P_j + H_j + F_j\right) \quad (50)$$

The objective function f_{cost} (Eq. (49)) is defined as the sum of annualized costs of investment (C_{inv,a_j}) and replacement (C_{rep,a_j}), and the cost of Operating & Maintenance ($C_{O\&Mj}$) multiplied by the design variable (D_j) of the j-th energy conversion and storage unit, plus the operating costs of the energy system, i.e. the cost related to the power (P_j), H_2 (H_j) and/or fuel (F_j), entering/exiting the energy system boundary. The objective function f_{CO_2} (Eq. (50)) is defined as the sum of the emissions deriving from the operation of the energy system, i.e. considering the $CO_{2,eq}$ emission referred to the energy flows entering/outgoing from the border of the energy system.

A linear combination of the cost objective function (Eq. (49)) and

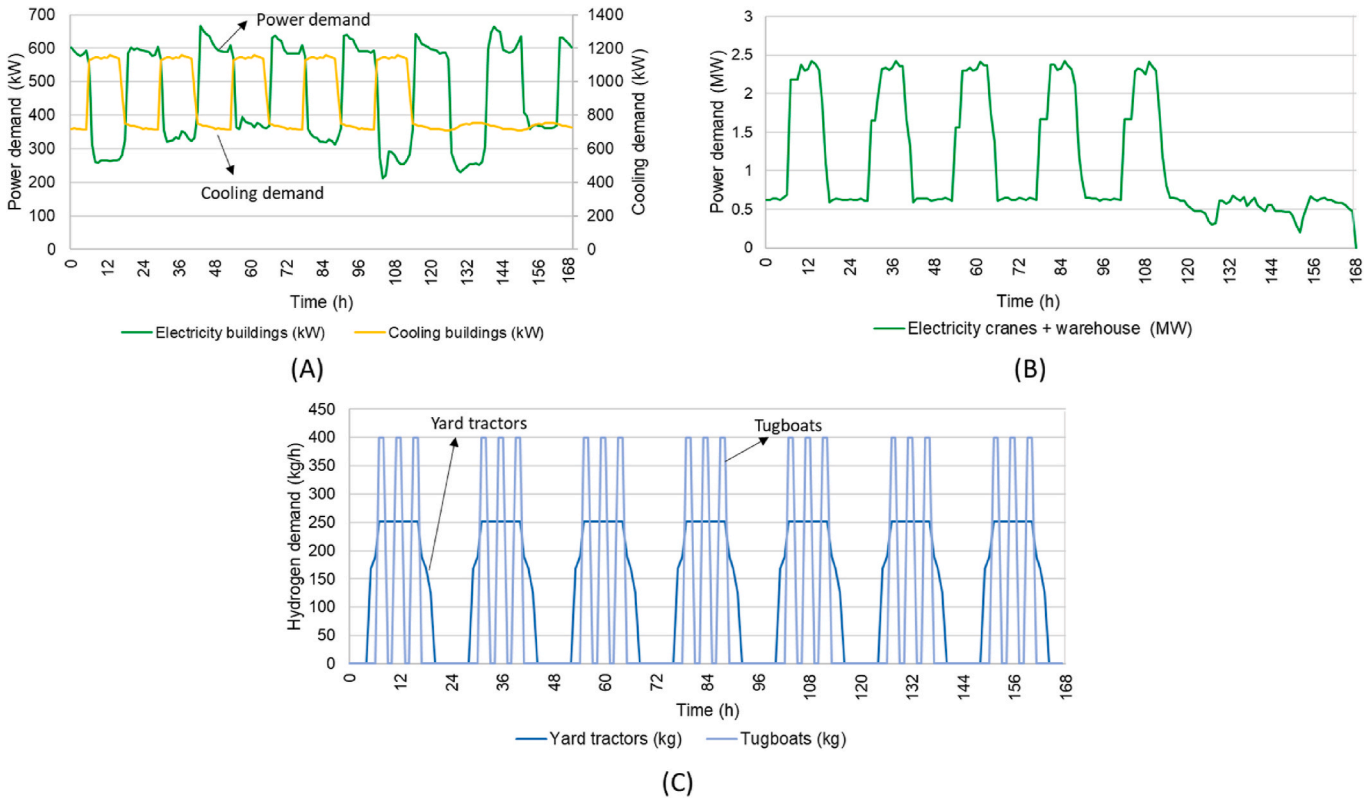

Fig. 1. Energy demand of the IPA over a typical working week: A) electric power (green line) and cooling (yellow line) demand required by port buildings, B) electric power demand required by warehouses and cranes, C) H_2 flow rate outgoing from the refuelling and bunkering stations used for the fleets of yard tractors and tugboats.

emission objective function (Eq. (50)) is defined. Different weights to the two objective functions are fixed, namely w_{cost} and w_{CO_2} in Eq. (51). The cost objective function is weighted with w_{cost}, here considered equal to 1. The emission objective function is weighted with w_{CO_2}, set equal to the value of the carbon tax. The combined objective function f_{MO} represents an economic objective function, in which the environmental impact (emissions derived from the operation) is considered as a cost.

$$f_{MO} = w_{cost} \cdot f_{cost} + w_{CO_2} \cdot f_{CO_2} \tag{51}$$

The annualized investment, replacement, operation and maintenance (O&M) costs are defined in Eqs. (52)–(54), where the i is the nominal interest rate, n is the assumed plant lifetime, LT_j is the assumed lifetime of the j-th unit, C_{inv_j} is the investment cost for the j-th unit. It is assumed that, at the end-of-life, the components are replaced with the same capital costs (Eq. (53)). $C_{O\&M_j}$ are calculated as dependent on the C_{inv,a_j} by the proportionality coefficient $c_{O\&M_j}$ (Eq. (54)).

$$C_{inv,a_j} = \frac{i \cdot (1+i)^n}{i \cdot (1+i)^n - 1} \cdot C_{inv_j} \tag{52}$$

$$C_{rep,a_j} = \frac{i \cdot (1+i)^n}{i \cdot (1+i)^n - 1} \cdot \frac{C_{inv_j}}{(1+i)^{LT_j}} \tag{53}$$

$$C_{O\&M_j} = c_{O\&M_j} \cdot C_{inv_j} \tag{54}$$

3. Energy system description

This section introduces the energy demand and the configuration of the analysed energy system. Section 3.1 addresses the analysis and synthesis of the energy required by the industry and port facilities located in the considered IPA. Section 3.2 presents a simplified schematic of the energy system and defines four energy system configurations alternative to the baseline energy system configuration, i.e. alternative to the assumed existing energy system of the IPA.

3.1. Analysis and synthesis of energy demands

Analysis and synthesis of the energy required by the industry and port facilities located in the considered IPA are performed. Four energy demands are considered and estimated, namely: (i) port buildings, (ii) electric cranes and warehouses, (iii) yard tractors and tugboats and (iv) industry. A typical work week is assumed to be representative of the annual operation of the energy system. Given the steadiness of the tropical climate throughout the year, with low seasonality characteristics of the weather (e.g., temperature and solar radiation), the weekly trend can be extended to the whole year with an acceptable uncertainties' magnitude.

The baseline energy system configuration (i.e. current energy system) considers the use of Diesel-fuelled yard tractors and tugboats, use NG for powering the CCGT, purchase of electric power to directly supply the port warehouses, cranes and building power demand and the vapour compressor chiller to provide cooling power to the buildings. Results of optimizations runs are then compared to this baseline configuration, underlighting the different design and operation of energy units and the related costs and carbon footprint. The operation of the CCGT power plant has a significant impact on the carbon emissions in the port area, accounting for 97.5 % of the total carbon emissions. The operative cost of the power plant is about 114.5 million € per year and is due to the purchase of natural gas from the natural gas grid, about 500 thousand tons of NG per year. The remaining 3 % of emissions are produced by the port operation, which includes diesel-powered yard tractors and tugboats, as well as the energy supply to cranes, buildings, and warehouses. The operation costs of the yard tractors and tugboats are about 7.2 and 5.1 million € per year, respectively, and are determined as the cost to

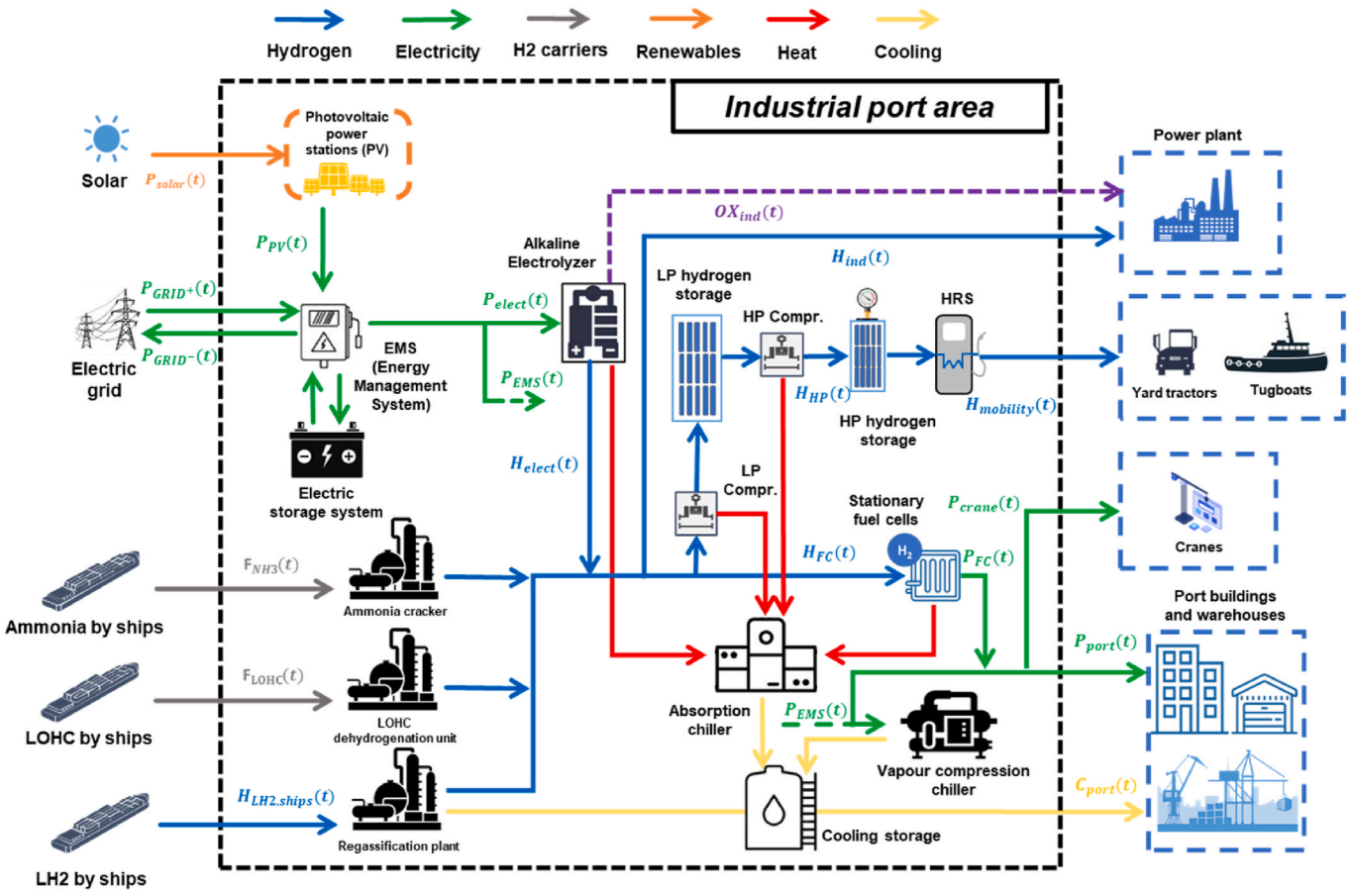

Fig. 2. Simplified schematic of the energy system proposed for the analysed IPA.

purchase Diesel oil as fuel for both yard tractors and tugboats. It is also assumed that the energy required by port buildings, warehouses and cranes, as well as the energy required by the VCC that meets the port's cooling demand, are both purchased from the electricity grid. Carbon footprints of the fossil fuels and of the power purchased from the grid are considered and are reported in the Supplementary Material. No investment, replacement and maintenance costs are considered for the baseline configuration.

Starting from the analysis of the current energy demand of the analysed IPA, the electric energy, cooling energy and H_2 demands considered in this analysis are represented in Fig. 1.

The energy demand of port buildings (i) is elaborated from Refs. [54,66]. Data are on an hourly basis for a typical work week. Fig. 1A shows the cooling (yellow line) and power (green line) demands of port buildings. The peak power demand occurs during night-time due to the peak demands of internal and external lighting systems. The cooling demand is required for air conditioning and shows a peak demand during the daily work hours, while a base load is required during the night to maintain lower temperatures inside the offices compared to the outdoor temperature.

The electricity required by electric cranes and warehouses (ii) is elaborated from Refs. [54,66]. Data are on an hourly basis for a typical work week. Cranes and warehouses have a power demand that follow the work shifts over the daily hours. About the 25 % of the peak power demand is required as base load over less energy-intensive hours due to the air conditioning demand and lighting system. Fig. 1B shows the power demand profile over a typical work week.

As for yard tractors and tugboats (iii), a conversion of the Diesel-powered powertrains to hybrid H_2 powertrains is proposed for these vehicles. To determine the appropriate number of vehicles to be powered by H_2, the decarbonization targets outlined in Ref. [67] is considered. H_2 demand of yard tractors and tugboats fleets is evaluated from data collecting in literature and based on existing applications [40,68]. Specifically, the plan involves converting six diesel-fuelled tugboats to H_2-fuelled ones, with a daily H_2 consumption of approximately 400 kg/day, and replacing 160 diesel-fuelled yard tractors with H_2-fuelled ones that consume around 21 kg/day. Each vehicle is assumed to be refuelled once per day. The refuelling schedule of each fleet are evaluated according to the characteristic of commercial HRS, i.e. the capacity in term of the maximum H_2 suppliable per hour and per day, as reported in Supplementary Material. Fig. 1C shows the weekly profile of the H_2 flow rates outgoing from the refuelling and bunkering stations for yard tractors and tugboats.

An industrial plant (iv) located nearby the considered port area is taken here as a potential H_2 user. A 600 MW advanced CCGT power plant is considered as a case study. Ref. [69] reports that CCGT is designed to be fuelled by a blend of 70%$_{vol}$ Natural Gas (NG) and 30%$_{vol}$ H_2, in volume. The CCGT will be modified to work with only H_2 (100%$_{vol}$ H_2) by 2026. Considering an 80 % utilization factor and a 60 % total energy efficiency, H_2 consumption is about 23 kt in 2023 and 210 kt in 2026. A constant hourly H_2 demand in a typical week is here considered. CCGT could be also fed directly by NH_3; however, this solution is not considered in the model.

3.2. Energy system configuration

The decarbonization strategies proposed for the IPA of Singapore are selected on the basis of guidelines and roadmaps defined in Refs. [67,70,71]. To match the energy demand required by the CCGT power plant and the port energy users with a lower carbon impact, new energy

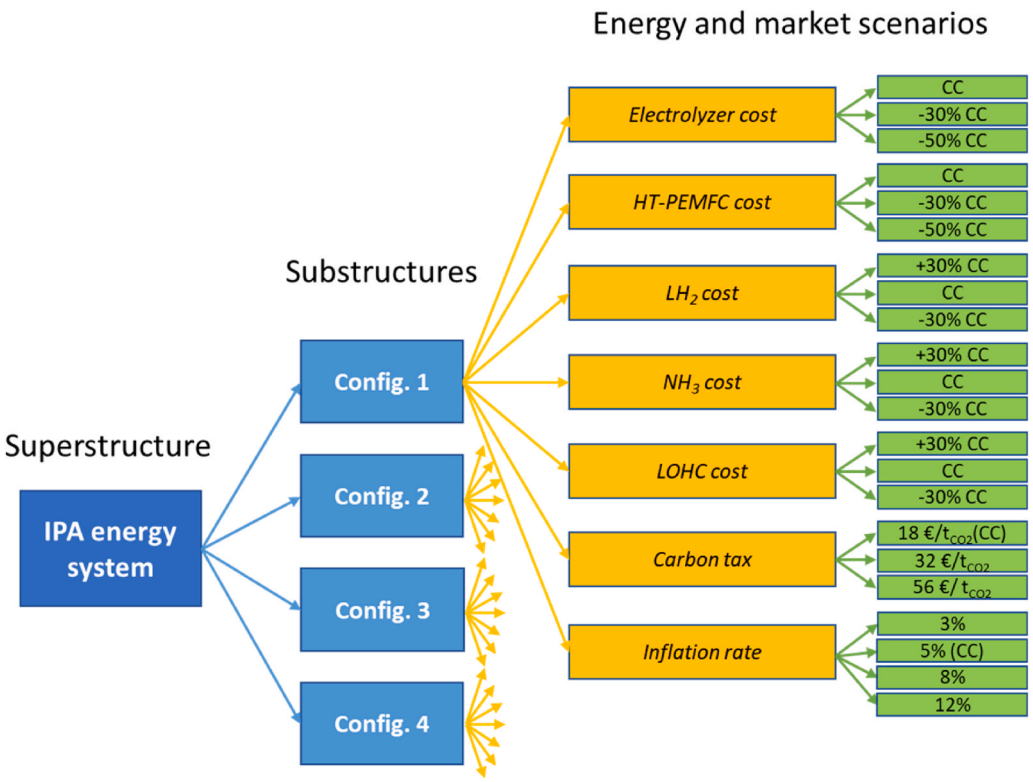

Fig. 3. Tree diagram for the definition of the energy and market frameworks of the analysis.

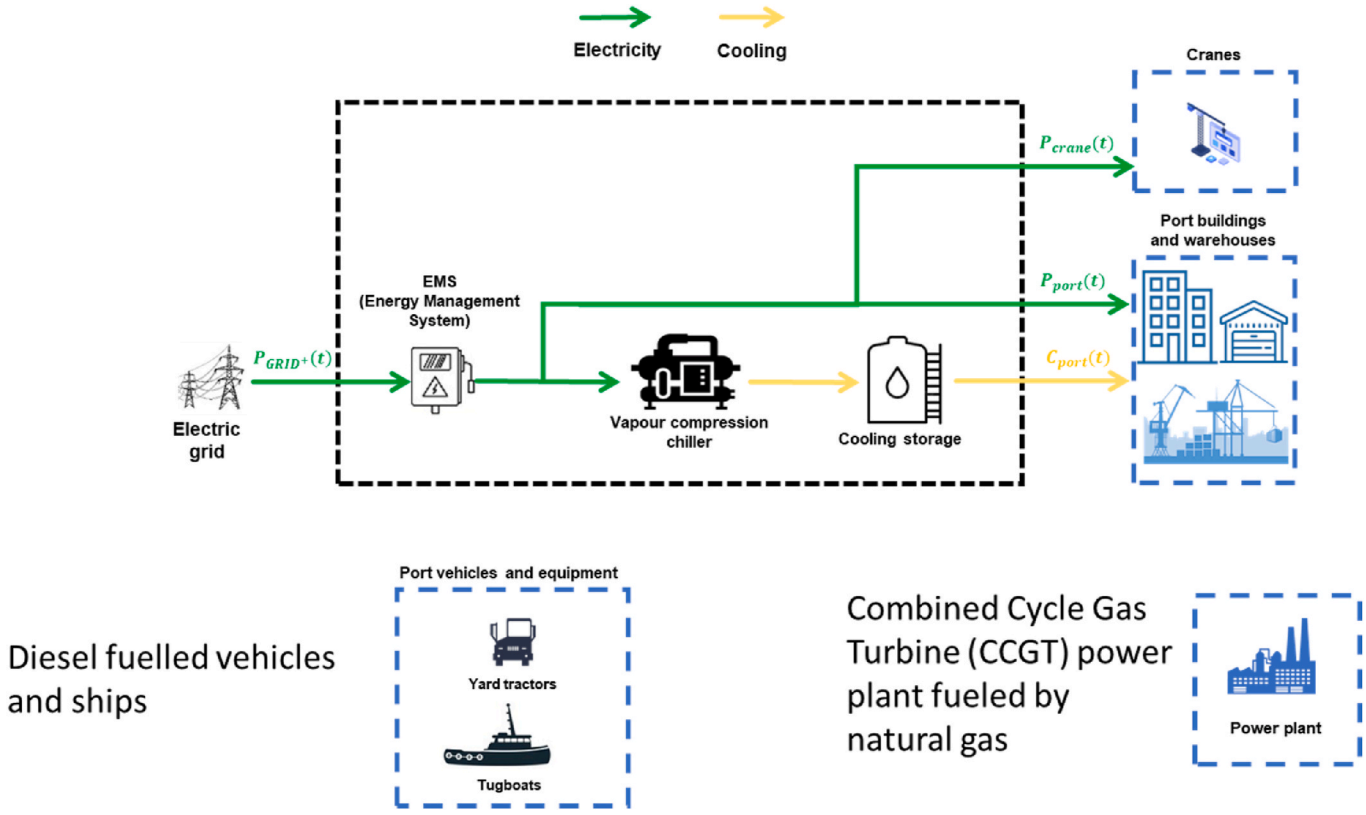

Fig. 4. Simplified schematic of the baseline configuration of the energy system.

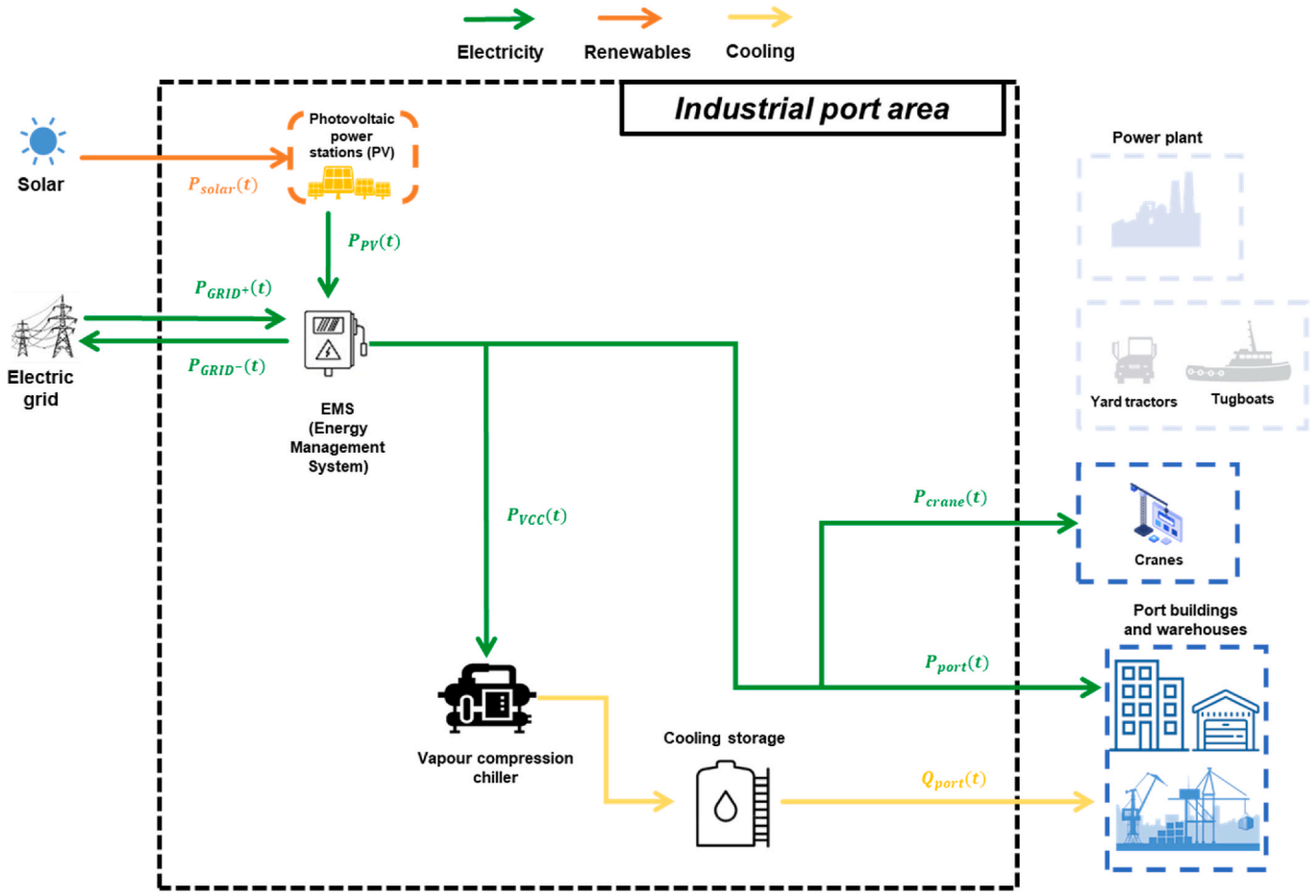

Fig. 5. Simplified schematic of the Config. 1. Energy conversion and storage units optimally selected by the optimization tool are included in the energy system configuration.

system configuration is proposed. In particular, the exploitation of local RES, electric and thermal energy storage systems, and technologies for H_2 import/production, storage and utilization have been investigated. Furthermore, the proposed energy system configuration comprises also technologies to convert LOHC, NH_3 and LH_2 into H_2 to be used for industry and mobility applications. The mentioned H_2 carriers are supposed to be imported via ship and stored in the IPA.

An alternative energy system configuration is proposed for the IPA. A simplified schematic of the alternative energy system configuration is depicted in Fig. 2, where arrows of different colour identify the flows of H_2 (blue lines), electric power (green lines), solar power (orange lines), heat power (red lines) and cooling power (yellow lines). Dashed lines mark the whole system boundaries (black dashed lines), the H_2/energy user units (blue dashed lines) and the available solar energy (orange dashed lines).

Electric power can be produced by the PV plant and/or purchased from the electric grid. Electricity can be stored in an electric storage system (LIB), sold to the grid, used to power the AEL, the VCC and/or supplied to match the electric power demand of port cranes, warehouses and buildings. Power can be also produced by stationary HT-PEMFC. H_2 can be produced by the AEL or imported as LOHC, NH_3 and LH_2 via ships. Technologies to convert H_2 carrier into pure gaseous H_2 are analysed, in particular, a dehydrogenation, a cracker and a regassification plant are considered for LOHC, NH_3 and LH_2, respectively. It is assumed that the gaseous H_2 has a high purity level (>99.95 %) and a pressure about 30 bar, equal to the pressure of H_2 leaving the AEL. H_2 at a pressure of 30 bar can be supplied directly to the CCGT power plant and to the stationary HT-PEMFC that are both fulfilled by H_2 at low pressure. If H_2 is directed to refuel yard tractors and tugboat has to be compressed till 820 bar in a two-pressure level H_2 compression stations. H_2 can be stored at a LP level (300 bar). Heat recovered from compressors, AEL and HT-PEMFC can be used by the ABC to provide cooling to the building and warehouses cooling demand and/or stored in a cooling storage. Alternatively, cooling can be generated by a VCC.

3.2.1. *Substructures of the proposed energy system configuration*

The impact of different decarbonization strategies for the energy system of the IPA is assessed by considering four different substructures derived from the superstructure shown in Fig. 2.

1) Configuration 1 (*Config. 1*) refers to the energy system substructure considering the port cooling and electricity power demand required by port buildings, warehouses and cranes;
2) Configuration 2 (*Config. 2*) refers to the energy system substructure considering the energy demand of Config. 1 plus the H_2 demand required by yard tractors and tugboats operating in the IPA.
3) Configuration 3 (*Config. 3*) refers to the energy system substructure considering the energy demand of Config. 2 plus the H_2 demand required by the CCGT power plant operating in the considered IPA. H_2 demand evaluated for the current scenario in 2023 is considered, assuming that gas turbines are fuelled by a 30 % H_2 blend with the natural gas.
4) Configuration 4 (*Config. 4*) is the same as Config. 3, except for the H_2 demand of the CCGT power plant. In this case, gas turbines are considered to be fuelled by 100 % H_2, as planned for the future operation in 2026.

A sensitivity analysis on the input parameters that most affect the

Table 1
Optimal design of energy conversion and storage units of configuration 1 in the differen energy and market scenarios.

	CC	−30 % CAPEX AEL	−50 % CAPEX AEL	−30 % CAPEX FC	−50 % CAPEX FC	+30 % cost LH_2	−30 % cost LH_2	+30 % cost LOHC	−30 % cost LOHC	+30 % cost NH_3	−30 % cost NH_3	Carbon tax 32 €/t	Carbon tax 56 €/t	Inflat. rate 3 %	Inflat. rate 8 %	Inflat. rate 12 %
PV (MWp)	**7.3**	**7.5**	**7.5**	**7.3**	**7.3**	**7.4**	**7.4**	**7.5**	**7.6**	**7.6**	**7.4**	**7.5**	**7.5**	**7.8**	**7.4**	**6.7**
Alkaline electrolyzer (kW)	0	0	0	0	0	0	0	0	0	0	0	0	0	0	0	0
FC (kW)	0	0	0	0	0	0	0	0	0	0	0	0	0	0	0	0
LP compressor (kW)	0	0	0	0	0	0	0	0	0	0	0	0	0	0	0	0
HP compressor (kW)	0	0	0	0	0	0	0	0	0	0	0	0	0	0	0	0
H_{LP} storage (kg)	0	0	0	0	0	0	0	0	0	0	0	0	0	0	0	0
H_{HP} storage (kg)	0	0	0	0	0	0	0	0	0	0	0	0	0	0	0	0
Refrigerator for HRS (kW)	0	0	0	0	0	0	0	0	0	0	0	0	0	0	0	0
Grid capacity (MW)	**2.3**	**2.3**	**2.3**	**2.3**	**2.3**	**2.3**	**2.3**	**2.3**	**2.3**	**2.3**	**2.3**	**2.3**	**2.3**	**2.3**	**2.3**	**2.3**
Vapour compr. chiller (kW)	**524.4**	**618.7**	**618.7**	**524.4**	**524.4**	**603.8**	**571.6**	**618.5**	**662.5**	**687.3**	**594.2**	**610.6**	**651.1**	**772.2**	**645.3**	**558.2**
Absorption chiller (kW)	0	0	0	0	0	0	0	0	0	0	0	0	0	0	0	0
Cooling energy storage (MWh)	**11.6**	**14.6**	**14.6**	**11.6**	**11.6**	**14.8**	**13.9**	**14.9**	**16.7**	**16.6**	**13.9**	**14.6**	**16.3**	**19.2**	**15.3**	**10.4**
NH_3 cracker (MW)	0	0	0	0	0	0	0	0	0	0	0	0	0	0	0	0
NH_3 storage (t)	0	0	0	0	0	0	0	0	0	0	0	0	0	0	0	0
LOHC dehydr. unit (t/h)	0	0	0	0	0	0	0	0	0	0	0	0	0	0	0	0
LOHC storage (t)	0	0	0	0	0	0	0	0	0	0	0	0	0	0	0	0
LH_2 vaporizer (t/h)	0	0	0	0	0	0	0	0	0	0	0	0	0	0	0	0
LH_2 storage (t)	0	0	0	0	0	0	0	0	0	0	0	0	0	0	0	0
Batt. Capacity (kWh)	0	0	0	0	0	0	0	0	0	0	0	0	0	0	0	0

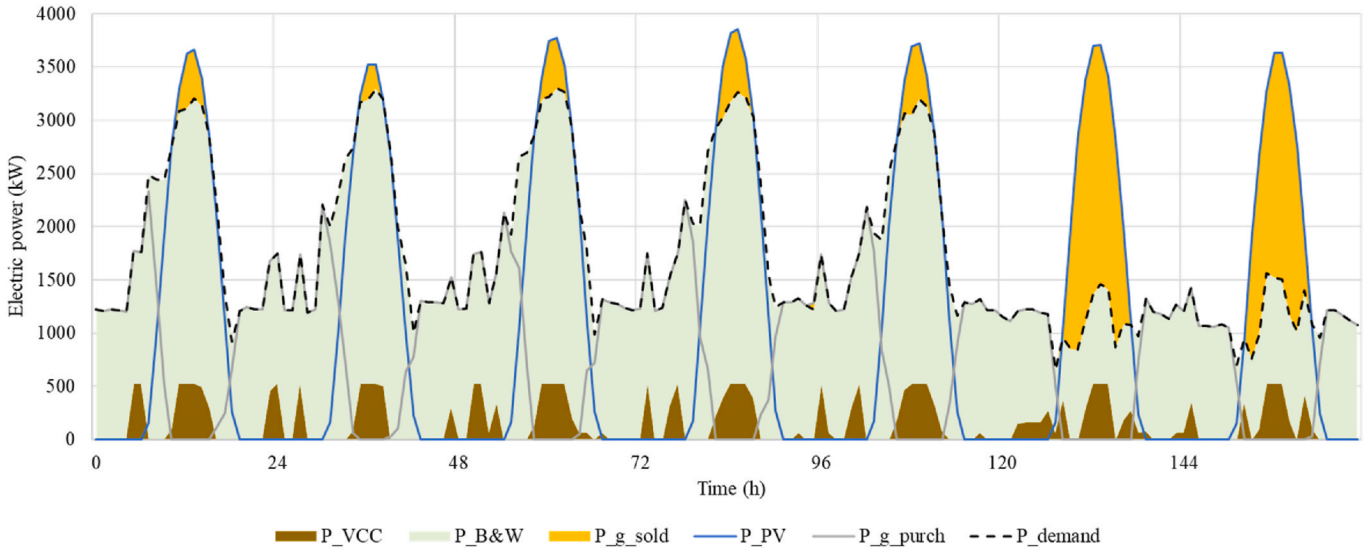

Fig. 6. Electric energy flows in the optimal operation of the energy system in the configuration 1.

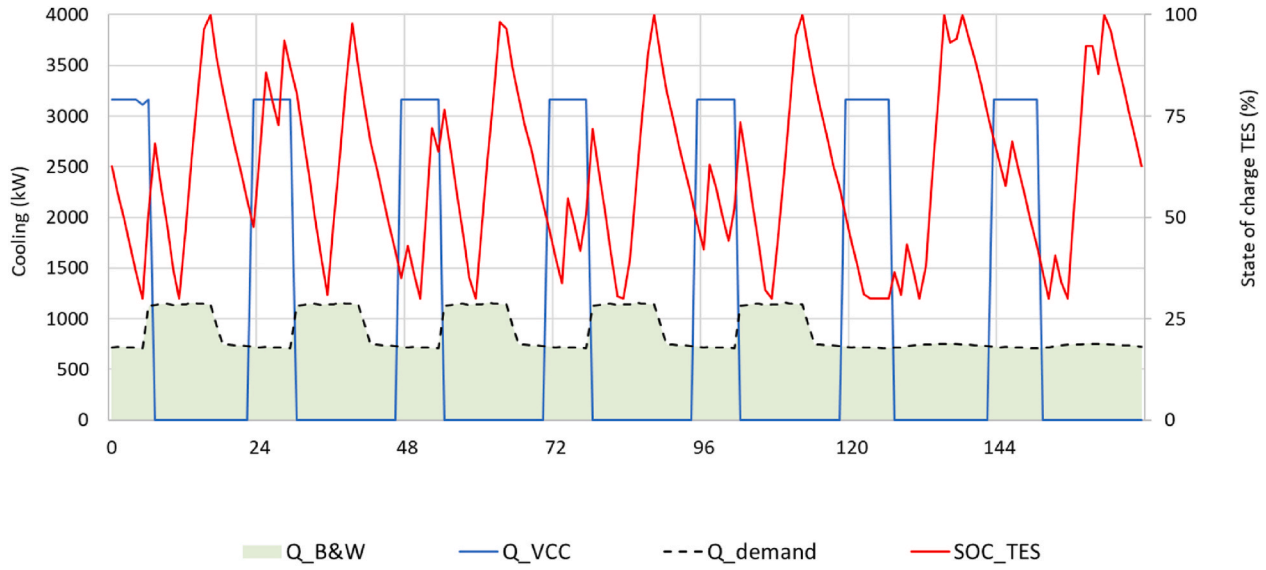

Fig. 7. Cooling energy flows in the optimal operation of the energy system in the configuration 1.

results of optimization is perfomed. In particular, it is analysed the possible variation of: i) AEL cost, ii) HT-PEMFC cost, iii) cost of imported LH_2, iv) cost of imported NH_3, v) cost of imported LOHC, vi) value of the carbon tax, and vii) value of the inflation rate. A simplified tree diagram presenting the different market considered for each of the four substructures is represented in Fig. 3. As for the AEL cost (i), a −30 % and −50 % reduction of the current cost is considered. The same possible reduction of cost is investigated for the cost of HT-PEMFC (ii). For the cost of imported LH_2 (iii), NH_3 (iv), and LOHC (v), a +30 % increase and −30 % decrease of the H_2 carriers cost are investigated. The carbon tax estimated by the National Climate Change Secretariat Singapore from 2024 to 2030 is here considered [72]. In particular, three different prices of the carbon tax (vi) are here considered and use in the optimizations: 18 €/$tCO_{2,eq}$ (carbon tax estimate in 2024–2025, and here considered as the current value), 32 €/$tCO_{2,eq}$ (in 2026–2027), and 56 €/$tCO_{2,eq}$ (by 2030). As for the inflation rate (vii), four different values are considered: 3 %, 5 %, 8 % and 12 %.

The sensitivity analysis is carried out considering the variation of one parameter at a time, when the other parameters are posed equal to the current values (Current Case, CC in Fig. 3). In this way, sixteen optimizations runs are performed for each substructure, for a total of sixty-four optimizations runs.

4. Results and discussion

The results achieved by means of the proposed optimization algorithm for the different substructures of the Singapore's IPA are presented in the following subsections. The design and the operation of the energy system components throughout a typical working week are presented and compared for each substructure and each energy-market scenario. Environmental techno-economic assessment of the distinct substructures compared with the baseline configuration of the energy system (Config. 0, represented in Fig. 4) are quantitatively evaluated and discussed.

The results of optimization are subdivided into four subsections: Config. 1 in Section 4.1, Config. 2 in Section 4.2, Config. 3 in Section 4.3 and Config. 4 in Section 4.4. In Section 4.5, results of different substructures are compared and discussed.

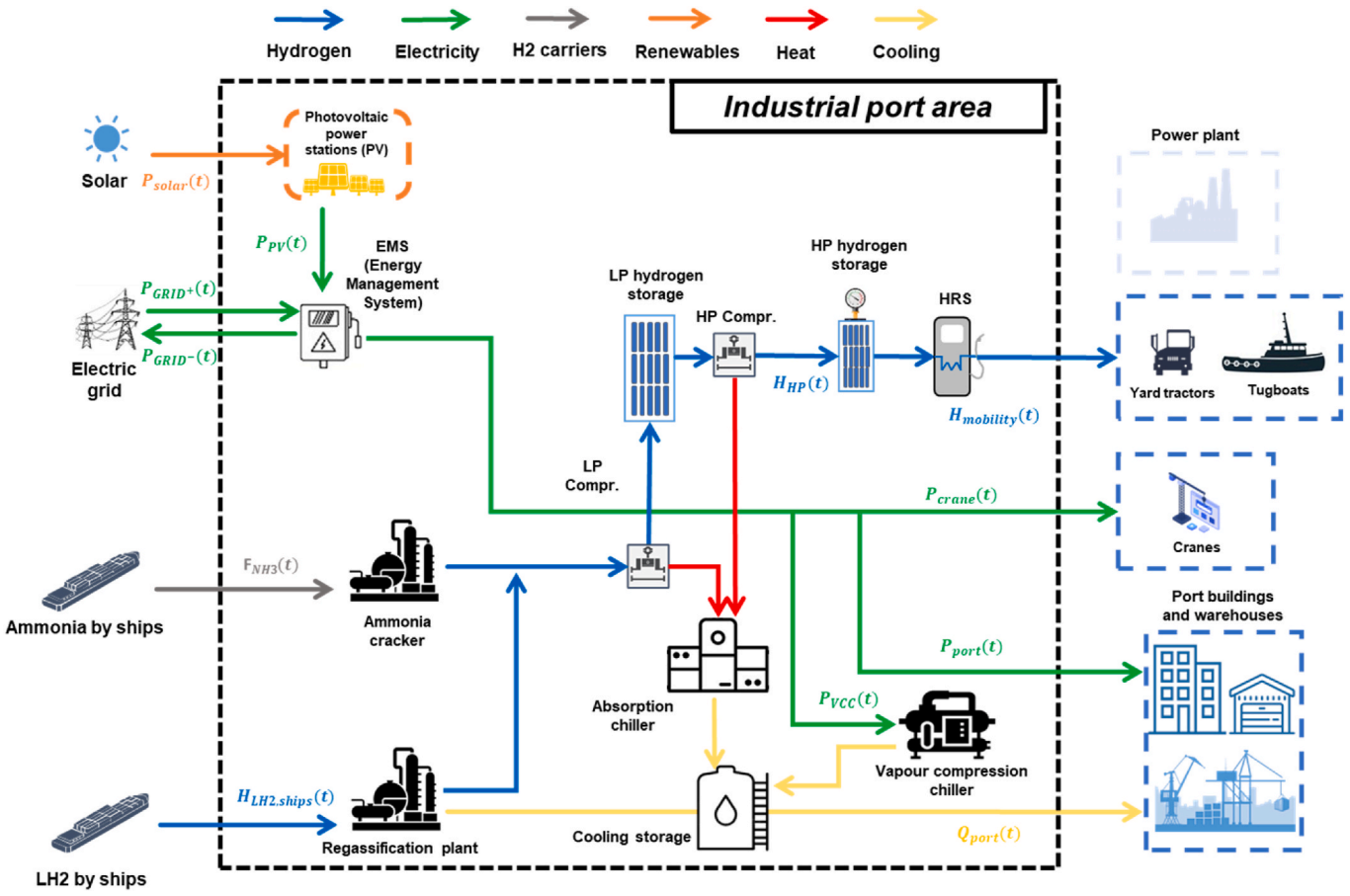

Fig. 8. Simplified schematic of the Config. 2. Energy conversion and storage units optimally selected by the optimization tool are included in the energy system configuration.

4.1. Substructure configuration 1

This subsection reports the optimization results of the substructure considering the electric and cooling demand required by port warehouses, buildings and cranes (Config. 1 in Section 3.2). The set of energy conversion and storage units chosen as optimal solution in the current energy and market scenario (referred as CC in Fig. 3) is represented in Fig. 5. The optimal design of the components in the CC is reported in Table 1. The optimal operation of the energy system over a work week is represented in Figs. 6 and 7, which show the electricity energy flows and the cooling energy flows, respectively.

In the CC, the optimal design of the substructure Config. 1 envisages the installation of a PV plant of approximately 7.3 MW_P, designed to cover the energy demand of the port buildings, warehouses, cranes and the VCC. Conversely, the optimization algorithm does not select any BESS capacity in the optimal solution space due to the high capital cost of the electric energy storage system compared to selling the excess electricity produced by PV directly to the grid. Part of the energy is purchased from the grid to cover the energy required by users (especially from the port lighting system) during the night, while part of the excess energy produced by the PV system is sold to the grid during peak energy production hours. The amount of energy sold to the grid is particularly high at weekends (Saturday and Sunday) when a lower electricity and cooling demand is required by the IPA.

A 524 kW_{el} VCC and a 11.6 MWh_{th} TES are installed to provide the cooling demand required by the port. The VCC operates when PV energy is available, while TES (charged during the hours of daylight) provides energy during the night.

4.1.1. Sensitivity analysis of configuration 1

A sensitivity analysis is performed to investigate the effect that input parameters has on the optimal design and operation of the system. As presented in Section 3.2 and represented in Fig. 3, for each substructure sixteen optimization cycles are performed, each time modifying one of the parameters considered in the analysis and leaving the others unchanged, i.e. considering values as defined in the CC. Table 1 reports the optimal design of the energy conversion and storage units for the different energy and market scenarios.

The results of the sensitivity analysis for Config. 1 show that there is no variation in the optimal choice of energy conversion and storage units, i.e. the components of the energy system are always the same even if they are slightly different in size.

The change in the inflation rate leads to a relatively larger change in the optimal component design. As the inflation rate increases, there is a decrease in the volume of the TES, a decrease in the installed PV power and a decrease in the power of the VCC, which is supplied by an increasing amount of energy purchased from the grid. For the other energy and market scenarios, the optimal component design undergoes slight variations due not to the different energy and market conditions (the parameters are in these cases considered ineffective on the optimization result), but to the value of the deviation (1 %) allowed for the minimisation of the objective function. In this case, although the design of the components changes, the overall system cost remains approximately the same.

4.2. Substructure configuration 2

This subsection reports the optimization results of the substructure considering the electric and cooling demand required by port

Table 2
Optimal design of energy conversion and storage units of configuration 2 in the differen energy and market scenarios.

	CC	−30 % CAPEX AEL	−50 % CAPEX AEL	−30 % CAPEX FC	−50 % CAPEX FC	+30 % cost LH_2	−30 % cost LH_2	+30 % cost LOHC	−30 % cost LOHC	+30 % cost NH_3	−30 % cost NH_3	Carbon tax 32 €/t	Carbon tax 56 €/t	Inflat. rate 3 %	Inflat. rate 8 %	Inflat. rate 12 %
PV (MWp)	**10.4**	**10.4**	**10.2**	**10.4**	**10.4**	**10.7**	**9.6**	**10.3**	**9.0**	**9.6**	**10.5**	**10.1**	**10.4**	**10.5**	**9.7**	**9.3**
Alkaline electrolyzer (kW)	0	0	0	0	0	0	0	0	0	0	0	0	0	0	0	0
FC (kW)	0	0	0	0	0	0	0	0	0	0	0	0	0	0	0	0
LP compressor (kW)	**797.0**	**799.2**	**667.1**	**797.0**	**797.0**	**797.0**	**510.9**	**793.6**	**441.0**	**510.9**	**794.0**	**647.6**	**796.9**	**800.5**	**721.3**	**661.5**
HP compressor (kW)	**275.4**	**275.4**	**275.4**	**275.4**	**275.4**	**275.4**	**275.4**	**275.4**	**275.4**	**275.4**	**275.4**	**297.1**	**275.4**	**275.4**	**275.4**	**275.4**
H_{LP} storage (kg)	**844.3**	**495.1**	**2044.8**	**844.3**	**844.3**	**671.4**	**2624.2**	**587.2**	**2932.1**	**2624.2**	**692.9**	**1364.0**	**676.2**	**1247.1**	**1220.9**	**1655.1**
H_{HP} storage (kg)	**574.3**	**731.6**	**1217.1**	**574.3**	**574.3**	**571.4**	**571.4**	**693.4**	**1081.4**	**571.4**	**571.4**	**963.2**	**626.7**	**615.7**	**571.4**	**571.4**
Refrigerator for HRS (kW)	**176.8**	**176.8**	**176.8**	**176.8**	**176.8**	**176.8**	**176.8**	**176.8**	**176.8**	**176.8**	**176.8**	**176.8**	**176.8**	**176.8**	**176.8**	**176.8**
Grid capacity (MW)	**2.8**	**2.7**	**2.7**	**2.8**	**2.8**	**2.8**	**2.9**	**2.7**	**2.7**	**2.9**	**2.8**	**2.8**	**2.7**	**2.8**	**2.7**	**2.8**
Vapour compr. chiller (kW)	**436.7**	**541.8**	**444.7**	**436.7**	**436.7**	**546.8**	**200.9**	**523.0**	0	**200.9**	**449.3**	**401.8**	**537.6**	**478.2**	**202.9**	0
Absorption chiller (kW)	**832.0**	**1033.1**	**795.3**	**832.0**	**832.0**	**813.9**	**606.1**	**986.1**	**746.9**	**606.1**	**836.9**	**868.1**	**1010.0**	**867.0**	**759.3**	**852.1**
Cooling energy storage (MWh)	**6.4**	**6.9**	**5.3**	**6.4**	**6.4**	**6.9**	**1.6**	**6.5**	**2.9**	**1.6**	**6.4**	**4.4**	**6.9**	**5.8**	**4.1**	**4.4**
NH_3 cracker (MW)	**1000.0**	**1000.0**	**1000.0**	**1000.0**	**1000.0**	**1000.0**	0	**1000.0**	0	0	**1000.0**	**1000.0**	**1000.0**	**1000.0**	**1000.0**	**1000.0**
NH_3 storage (t)	**50.1**	**50.8**	**53.0**	**50.1**	**50.1**	**52.6**	0	**50.5**	0	0	**53.1**	**53.1**	**50.6**	**53.1**	**51.2**	**53.1**
LOHC dehydr. unit (t/h)	0	0	0	0	0	0	0	0	**341.3**	0	0	0	0	0	0	0
LOHC storage (t)	0	0	0	0	0	0	0	0	**55.3**	0	0	0	0	0	0	0
LH_2 vaporizer (t/h)	**100.0**	**100.3**	0	**100.0**	**100.0**	**100.0**	**320.6**	**100.0**	0	**320.6**	0	0	**100.0**	0	**100.0**	0
LH_2 storage (t)	**2.5**	**1.9**	0	**2.5**	**2.5**	**0.4**	**44.8**	**2.2**	0	**44.8**	0	0	**2.1**	0	**1.5**	0
Batt. Capacity (kWh)	0	0	0	0	0	0	0	0	0	0	0	0	0	0	0	0

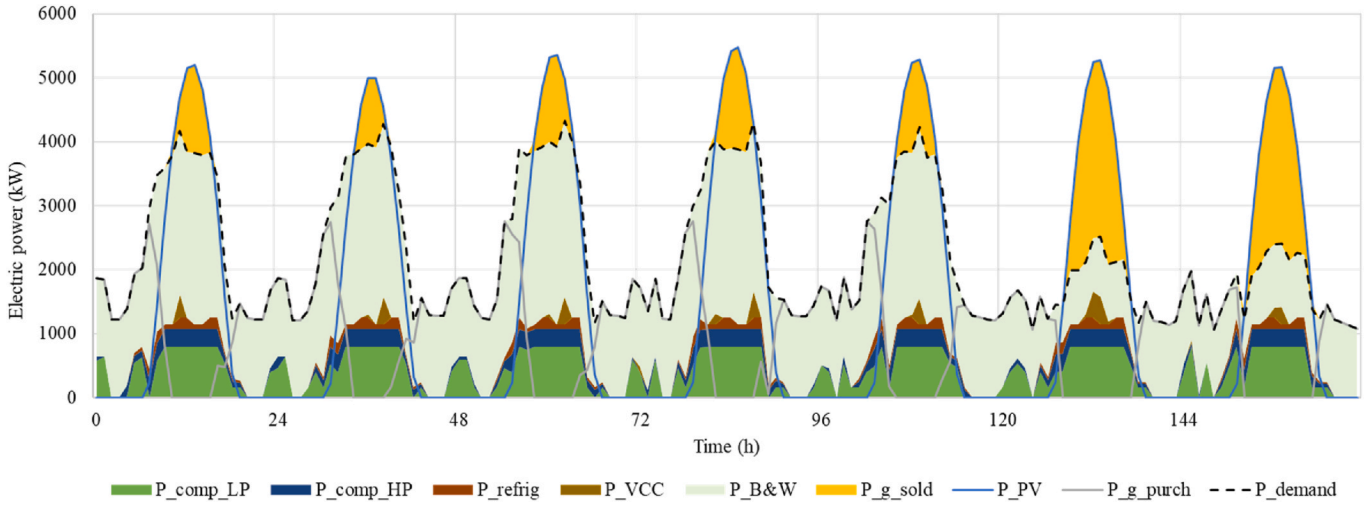

Fig. 9. Electric energy flows in the optimal operation of the energy system in the configuration 2.

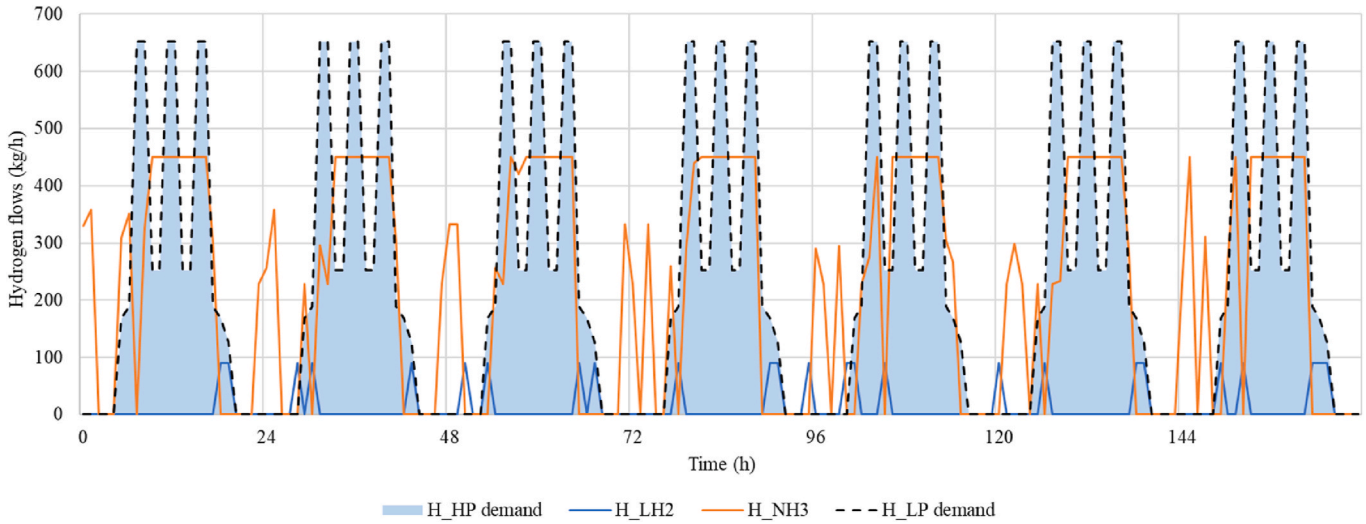

Fig. 10. H_2 flows in the optimal operation of the energy system in the configuration 2.

warehouses, buildings and cranes, and the H_2 demand required by the port fleets of yard tractors and tugboats (Config. 2 in Section 3.2). The set of energy conversion and storage units chosen as optimal solution in the current energy and market scenario (referred as CC in Fig. 3) is represented in Fig. 8. The optimal design of the components in the CC is reported in Table 2. The optimal operation of the energy system over a work week is represented in Figs. 9 and 10 reporting the electricity energy flows and the H_2 flows, respectively. Cooling and heating energy flows are represented in Figs. 11 and 12, respectively.

The H_2 required by tugboats and yard tractors is economically more convenient to be imported via ship as NH_3 (about 95 % of H_2 demand) and LH_2 (about 5 % of H_2 demand), while local H_2 production via electrolysis results to be not economically convenient as the LOHC import via ship. Part of the cooling recovered from the LH_2 regasification plant (about 1 % of the total port cooling demand) is used to meet the cooling demand of the port's warehouses and buildings. The remaining demand for cooling is fulfilled by a 437 kW_{el} VCC (about 14 % of cooling demand) and an 832 kW_{th} ABC (about 85 % of cooling demand). The latter is powered by the waste heat recovered from the operation of the two compression stations (797 kW_{el} of LP compressor and 275 kW_{el} of HP compressor). About 32 % of the total heat generated during the H_2 compression is dissipated through the heat dissipation unit. H_2 compressors and the VCC tend to operate when the power from the 10.4 MW_P PV is available. As resulted in Config. 1, the excess of power produced by the PV in the peak production hours and during weekends is sold to the grid and not stored in LIB.

4.2.1. *Sensitivity analysis of configuration 2*

As performed for configuration 1 (Section 4.11), a sensitivity analysis is performed to investigate the effect that input parameters has on the optimal design and operation of the system.

Table 2 reports the optimal design of the energy conversion and storage units for the different energy and market scenarios.

The parameters that do not substantially influence the design of energy conversion and storage units are the cost of the AEL, HT-PEMFC and carbon tax. As discussed in Section 4.1, a slight variation in the design of some energy units is due to the deviation allowed for the minimisation of the objective function (1 %). In this case, the design of the components changes, but the overall system cost remains approximately the same.

In general, AEL and HT-PEMFC are never chosen as optimal solutions in different energy and market scenarios, nor is LIB. NH_3 is not cost-effective to import by ship when the cost of LH_2 or LOHC is 30 % lower than CC, or when the cost of NH_3 is 30 % higher than CC. In the latter case, or also when the cost of LH_2 is 30 % lower, importing LH_2 is chosen as the optimal solution to cover the entire H_2 demand of tugboats

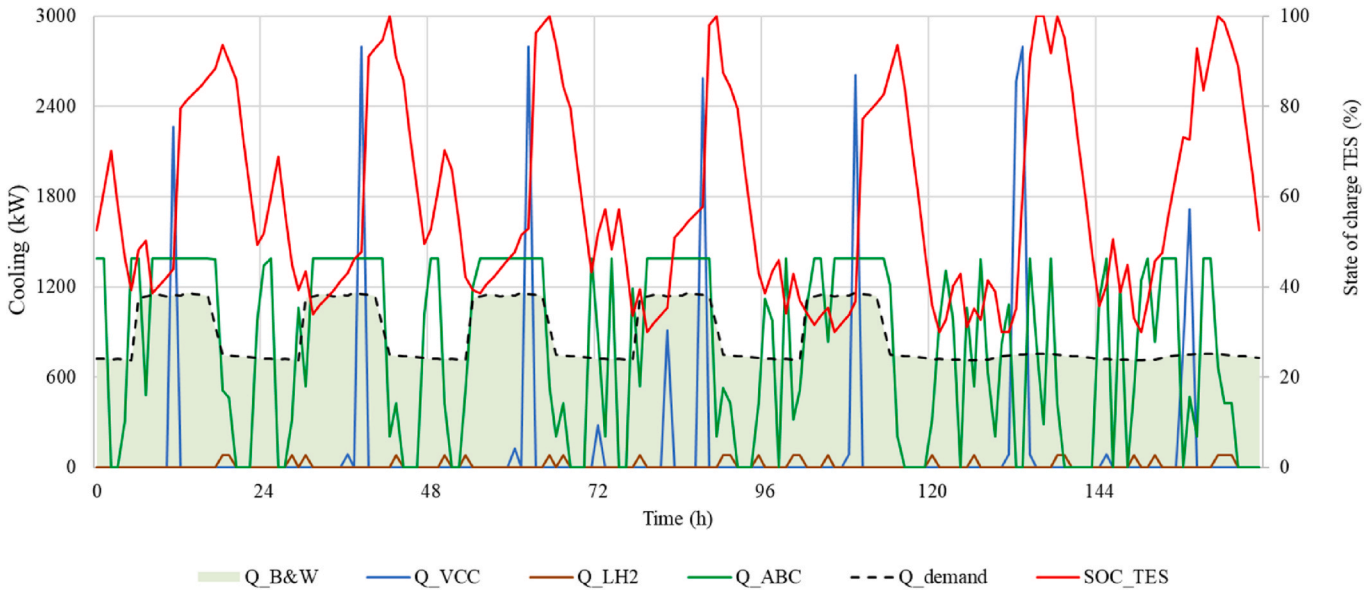

Fig. 11. Cooling energy flows in the optimal operation of the energy system in the configuration 2.

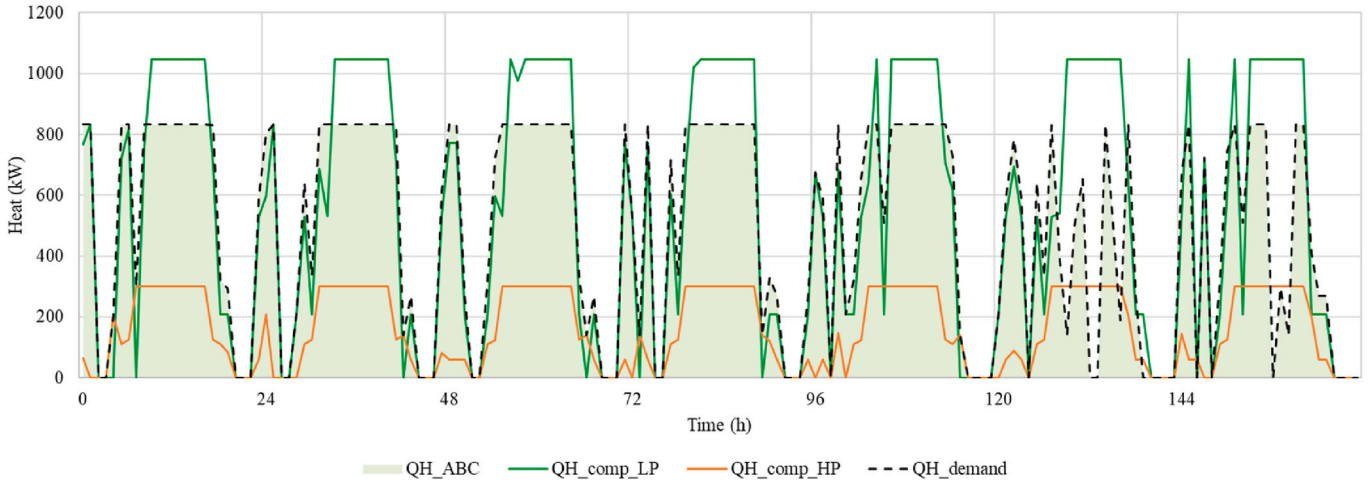

Fig. 12. Heating energy flows in the optimal operation of the energy system in the configuration 2.

and yard tractors. In addition, in this case due to the higher supply of LH_2, the cooling recovered from the regasification unit of LH_2 covers an important cooling demand of the port, significantly reducing the installed power of ABC and VCC compared to CC. LOHC is only imported when its cost is 30 % lower than CC, covering thus the entire H_2 demand. Changes in the inflation rate marginally affect the design of energy units, except for the VCC and ABC. In particular, the power output of the ABC tends to increase as the inflation rate increases, while the VCC installed power tends to decrease until it is no longer convenient to install when the inflation rate is 12 %.

4.3. Substructure configuration 3

This subsection reports the optimization results of the substructure considering the electric and cooling demand required by port warehouses, buildings and cranes, and the H_2 demand required by the port fleets of yard tractors and tugboats and, differently by configuration 2, by the CCGT plant in 2023 (Config. 3 in Section 3.2). The set of energy conversion and storage units chosen as optimal solution in the current energy and market scenario (referred as CC in Fig. 3) is represented in Fig. 13. The optimal design of the components in the CC is reported in Table 3. The optimal operation of the energy system over a work week is represented in the following figure. Fig. 14 shows the electricity energy flows, Fig. 15 the H_2 flows. Cooling and heating energy flows are represented in Figs. 16 and 17, respectively.

The optimization results show that the total H_2 demand (CCGT plant, port tugboats and yard tractors) of the IPA is covered by the NH_3 imported via ships. Respect to the Configuration 2, storage of NH_3 increased by approx one order of magnitude due to the higher demand of H_2 imposed by the CCGT. The heat recovered from the operation of the LP compressor (670 kWel) and HP compressor (275 kWel) can be supplied to the ABC, which can cover the entire cooling demand required by the port. About 19 % of the total heat generated during the H_2 compression is dissipated through the heat dissipation unit. Compressors tend to run when energy is produced by PV. H_2 converted by the NH_3 cracker is compressed and stored in the LP storage when it is not used directly to the CCGT plant, in order to limit the power installed for the cracker.

4.3.1. Sensitivity analysis of configuration 3

As performed for configuration 1 (Section 4.11), a sensitivity analysis is performed to investigate the effect that input parameters has on

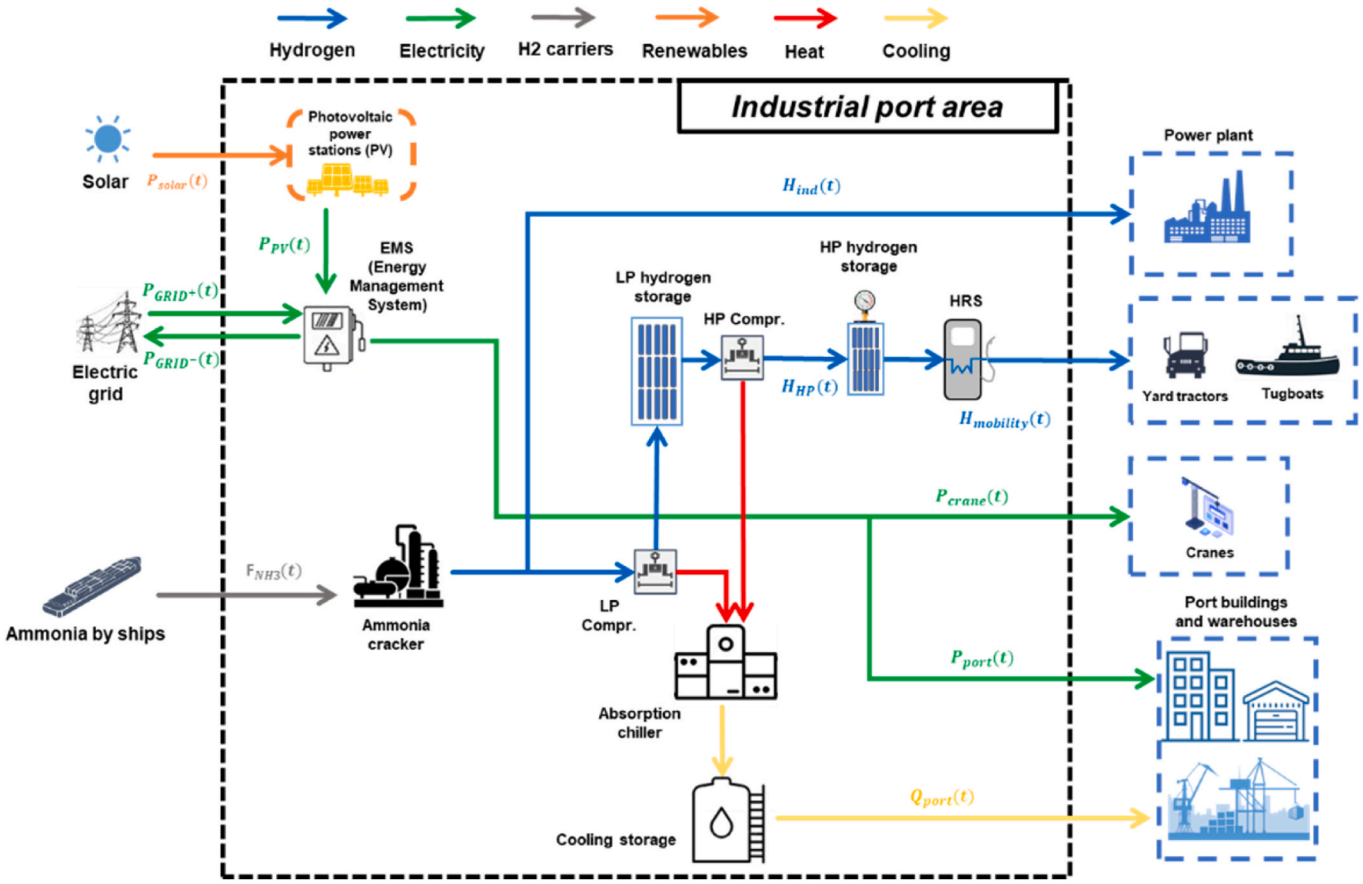

Fig. 13. Simplified schematic of the Config. 3. Energy conversion and storage units optimally selected by the optimization tool are included in the energy system configuration.

the optimal design and operation of the system.

Table 3 reports the optimal design of the energy conversion and storage units for the different energy and market scenarios.

Sensitivity analysis on model input parameters of Config. 3 outlines that the installation of FC and LIB is not a cost-effective solution for all the sixteen sensitivity scenarios. Whereas LOHC comes into play when its cost is 30 % lower than the CC, the import of LH_2 results to be in the optimal solution space when its cost is assumed to be 30 % lower than the CC. The same outcome will be also achieved with a 30 % higher cost of NH_3.

In scenarios where the LH_2 cost is 30 % lower than CC or the NH_3 cost is 30 % higher, NH_3 still covers part of the H_2 required by the IPA and part is instead produced locally via electrolysis. In fact, the installation of an AEL with a power ranging from 276.9 to 435.8 kW_{el} is considered. AEL is convenient to be installed also when its costs is 30 % (and 50 %) lower than the CC, when carbon tax is 56 €/$tCO_{2,eq}$ and when the inflation rate is 12 %. In the presence of higher values of the carbon tax or of the inflation rate, the excess energy produced by PV is indeed cheaper to use to produce H_2 than to sell to the grid.

Most of the cooling demand is covered by the cooling generated by the ABC powered by the heat recovered from the compressors. When LH_2 is imported, cooling recovered from the regassification covers the port demand. In these cases, a cold TES with higher capacity respect to the other scenarios is convenient to be installed to restrict the installed power capacity of the regasification unit.

4.4. Substructure configuration 4

This subsection reports the optimization results of the substructure considering the electric and cooling demand required by port warehouses, buildings and cranes, and the H_2 demand required by the port fleets of yard tractors and tugboats and by the CCGT plant in 2026 (Config. 4 in Section 3.2). The set of energy conversion and storage units chosen as optimal solution in the current energy and market scenario (referred as CC in Fig. 3) is represented in Fig. 18. The optimal design of the components in the CC is reported in Table 4. The optimal operation of the energy system over a work week is represented in the following figure. Fig. 19 shows the electricity energy flows, Fig. 20 the H_2 flows. Cooling and heating energy flows are represented in Figs. 21 and 22, respectively.

The optimization results of Config. 4 in the CC show that the IPA H_2 demand is fully covered by the NH_3 imported via ships. The waste heat recovered from the operation of the LP compressor (732 kW_{el}) and HP compressor (275 kW_{el}) is supplied to the ABC to fulfil the entire cooling demand required by the port. About 19 % of the total heat generated during the H_2 compression is dissipated through the heat dissipation unit. Similar to Config.3, the H_2 compressors tends to operate at high loads whenever there is a significant availability of electricity produced by the PV. In order to restrict the power capacity of the cracker, the H_2 converted from the NH_3 cracker is compressed and stored in the LP storage whenever there is no demand from the CCGT plant.

4.4.1. Sensitivity analysis of configuration 4

As performed for configuration 1 (Section 4.11), a sensitivity analysis is performed to investigate the effect of the input parameters on the optimal design and operation of the system.

Table 4 reports the optimal design of the energy conversion and storage units for the different energy and market scenarios.

The sensitivity analysis outlines that in any scenario AEL, FC, VCC and LIB are not cost-effective solutions for the installation. As shown in

Table 3
Optimal design of energy conversion and storage units of configuration 3 in the differen energy and market scenarios.

	CC	−30 % CAPEX AEL	−50 % CAPEX AEL	−30 % CAPEX FC	−50 % CAPEX FC	+30 % cost LH_2	−30 % cost LH_2	+30 % cost LOHC	−30 % cost LOHC	+30 % cost NH_3	−30 % cost NH_3	Carbon tax 32 €/t	Carbon tax 56 €/t	Inflat. rate 3 %	Inflat. rate 8 %	Inflat. rate 12 %
PV (MWp)	**9.3**	**10.3**	**10.1**	**9.3**	**9.3**	**9.4**	**8.8**	**9.3**	**14.3**	**9.4**	**9.4**	**10.0**	**10.4**	**9.6**	**9.2**	**9.6**
Alkaline electrolyzer (kW)	0	**276.9**	**450.2**	0	0	**435.8**	0	0	0	**421.2**	0	0	**427.2**	0	0	**392.9**
FC (kW)	0	0	0	0	0	0	0	0	0	0	0	0	0	0	0	0
LP compressor (kW)	**696.9**	**756.7**	**663.7**	**696.9**	**696.9**	**598.9**	**554.3**	**735.5**	**481.2**	**543.1**	**602.6**	**787.0**	**639.2**	**777.4**	**662.1**	**554.7**
HP compressor (kW)	**274.8**	**260.4**	**275.4**	**274.8**	**274.8**	**275.4**	**275.4**	**274.2**	**275.4**	**289.8**	**275.4**	**270.8**	**275.4**	**267.5**	**275.4**	**275.4**
H_{LP} storage (kg)	**1383.5**	**436.2**	**1571.3**	**1383.5**	**1383.5**	**2013.1**	**1850.0**	**1089.8**	**2879.4**	**2356.7**	**2082.3**	**276.8**	**1823.1**	**377.2**	**1650.7**	**2341.0**
H_{HP} storage (kg)	**586.1**	**1098.7**	**645.7**	**586.1**	**586.1**	**571.4**	**1217.1**	**599.5**	**656.0**	**773.9**	**571.4**	**1038.6**	**571.4**	**878.9**	**571.4**	**571.4**
Refrigerator for HRS (kW)	**176.8**	**176.8**	**176.8**	**176.8**	**176.8**	**176.8**	**176.8**	**176.8**	**176.8**	**176.8**	**176.8**	**176.8**	**176.8**	**176.8**	**176.8**	**176.8**
Grid capacity (MW)	**2.7**	**2.8**	**2.7**	**2.7**	**2.7**	**2.9**	**2.6**	**2.7**	**4.0**	**2.9**	**2.7**	**2.6**	**2.9**	**2.8**	**2.7**	**3.0**
Vapour compr. chiller (kW)	0	**153.3**	0	0	0	0	0	0	**84.9**	0	0	**433.0**	0	0	0	0
Absorption chiller (kW)	**900.4**	**488.6**	**794.5**	**900.4**	**900.4**	**769.0**	0	**938.8**	**736.3**	0	**743.2**	**759.0**	**754.0**	**1034.3**	**858.6**	**693.3**
Cooling energy storage (MWh)	**4.6**	**2.9**	**3.0**	**4.6**	**4.6**	**4.1**	**352.8**	**4.4**	**1.9**	**356.2**	**4.7**	**5.6**	**3.6**	**6.8**	**3.8**	**3.4**
NH_3 cracker (MW)	**4019.4**	**4060.3**	**3988.9**	**4019.4**	**4019.4**	**3946.6**	**3501.7**	**4048.1**	**3501.7**	**1000.0**	**3949.4**	**4086.4**	**3971.0**	**4079.3**	**3993.6**	**3908.6**
NH_3 storage (t)	**641.3**	**640.7**	**639.9**	**641.3**	**641.3**	**640.9**	**5.6**	**641.3**	**3.5**	**1.8**	**640.9**	**641.3**	**640.5**	**641.3**	**641.3**	**640.4**
LOHC dehydr. unit (t/h)	0	0	0	0	0	0	0	0	0	0	0	0	0	0	0	0
LOHC storage (t)	0	0	0	0	0	0	0	0	0	0	0	0	0	0	0	0
LH_2 vaporizer (t/h)	0	0	**1.0**	0	0	0	**3.3**	0	0	**3.3**	0	0	0	0	0	0
LH_2 storage (t)	0	0	**0.7**	0	0	0	**536.8**	0	0	**540.1**	0	0	0	0	0	0
Batt. Capacity (kWh)	0	0	0	0	0	0	0	0	0	0	0	0	0	0	0	0

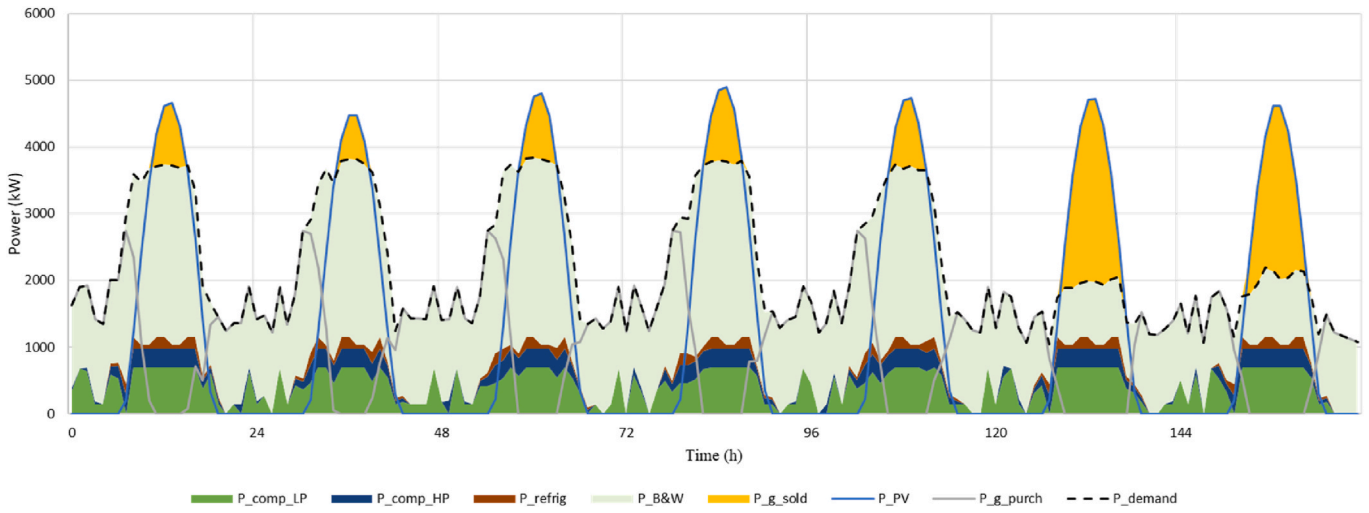

Fig. 14. Electric energy flows in the optimal operation of the energy system in the configuration 3.

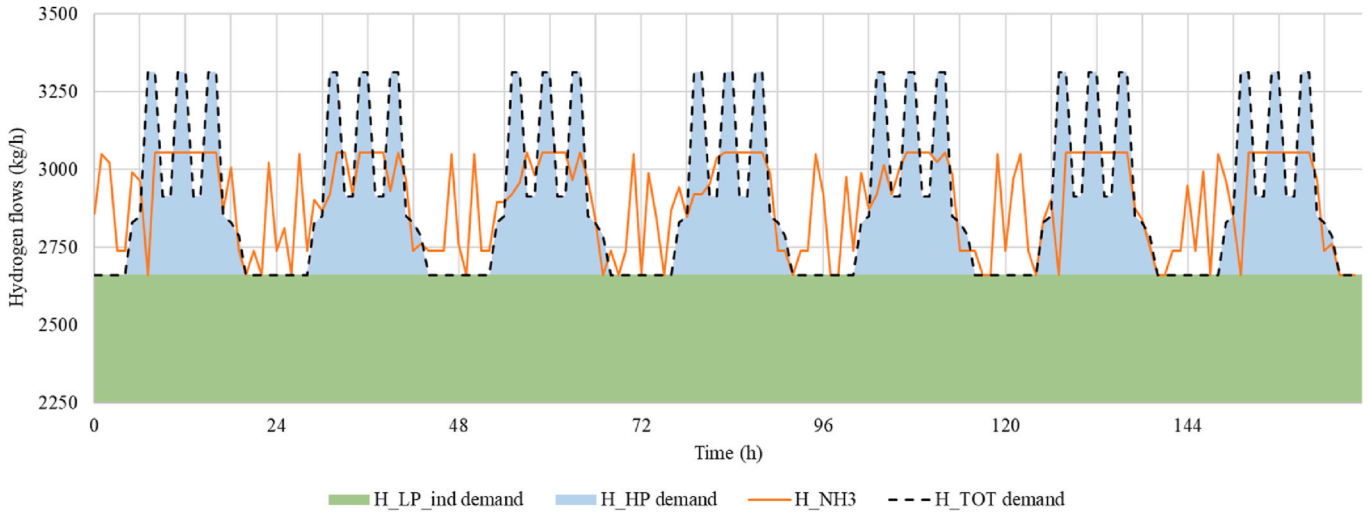

Fig. 15. H_2 flows in the optimal operation of the energy system in the configuration 3.

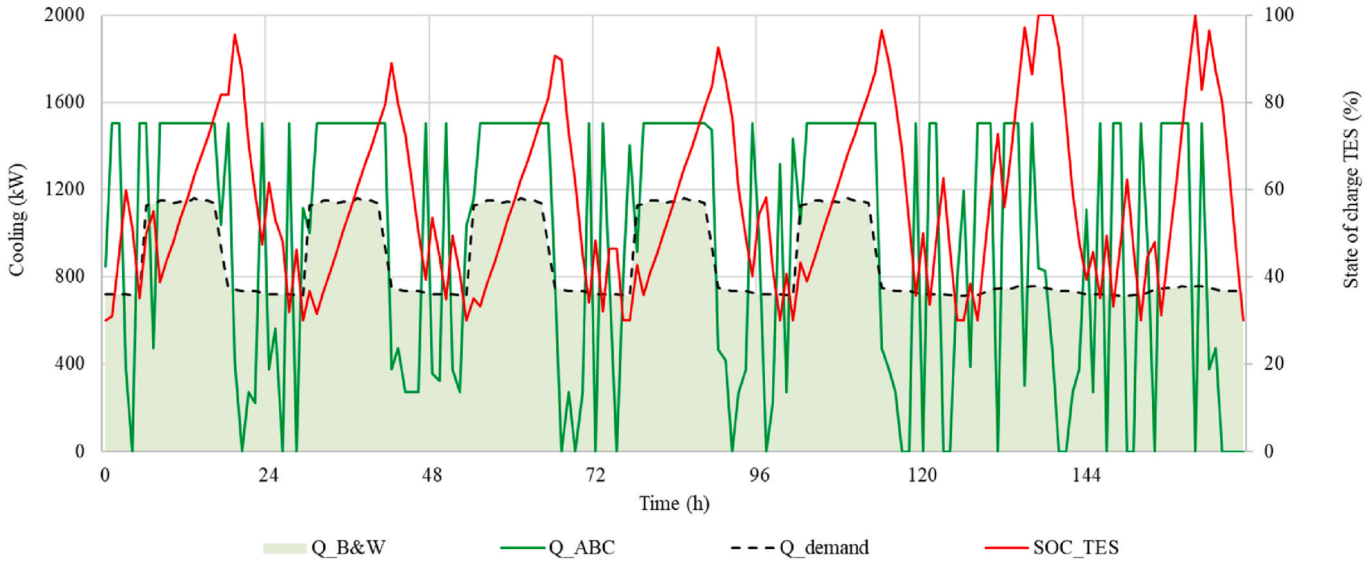

Fig. 16. Cooling energy flows in the optimal operation of the energy system in the configuration 3.

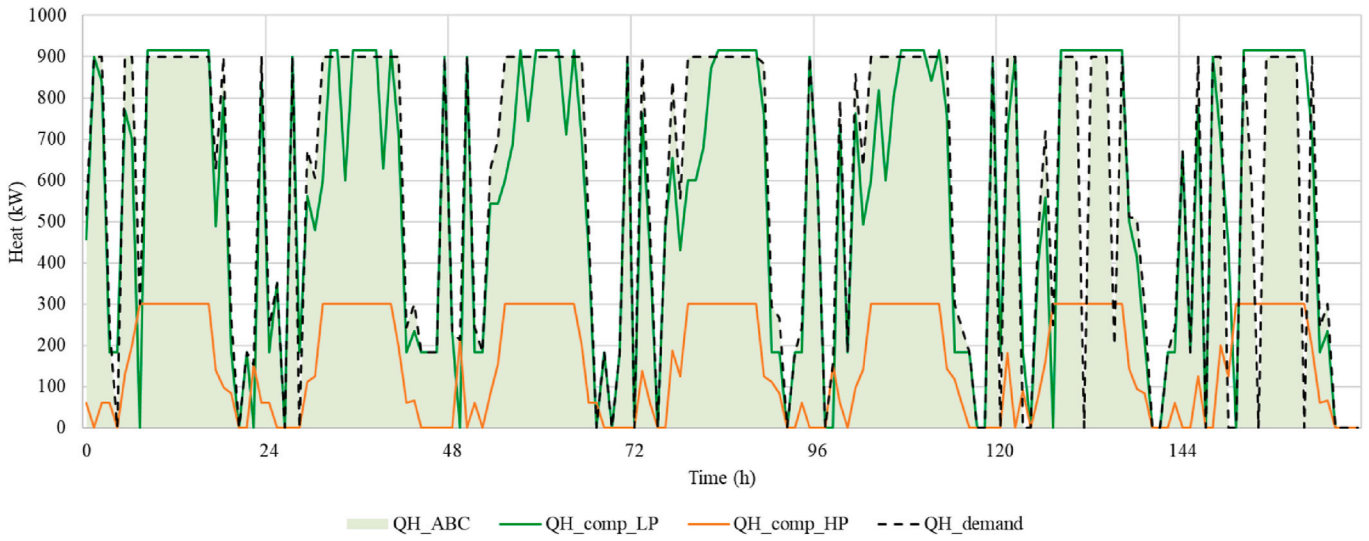

Fig. 17. Heating energy flows in the optimal operation of the energy system in the configuration 3.

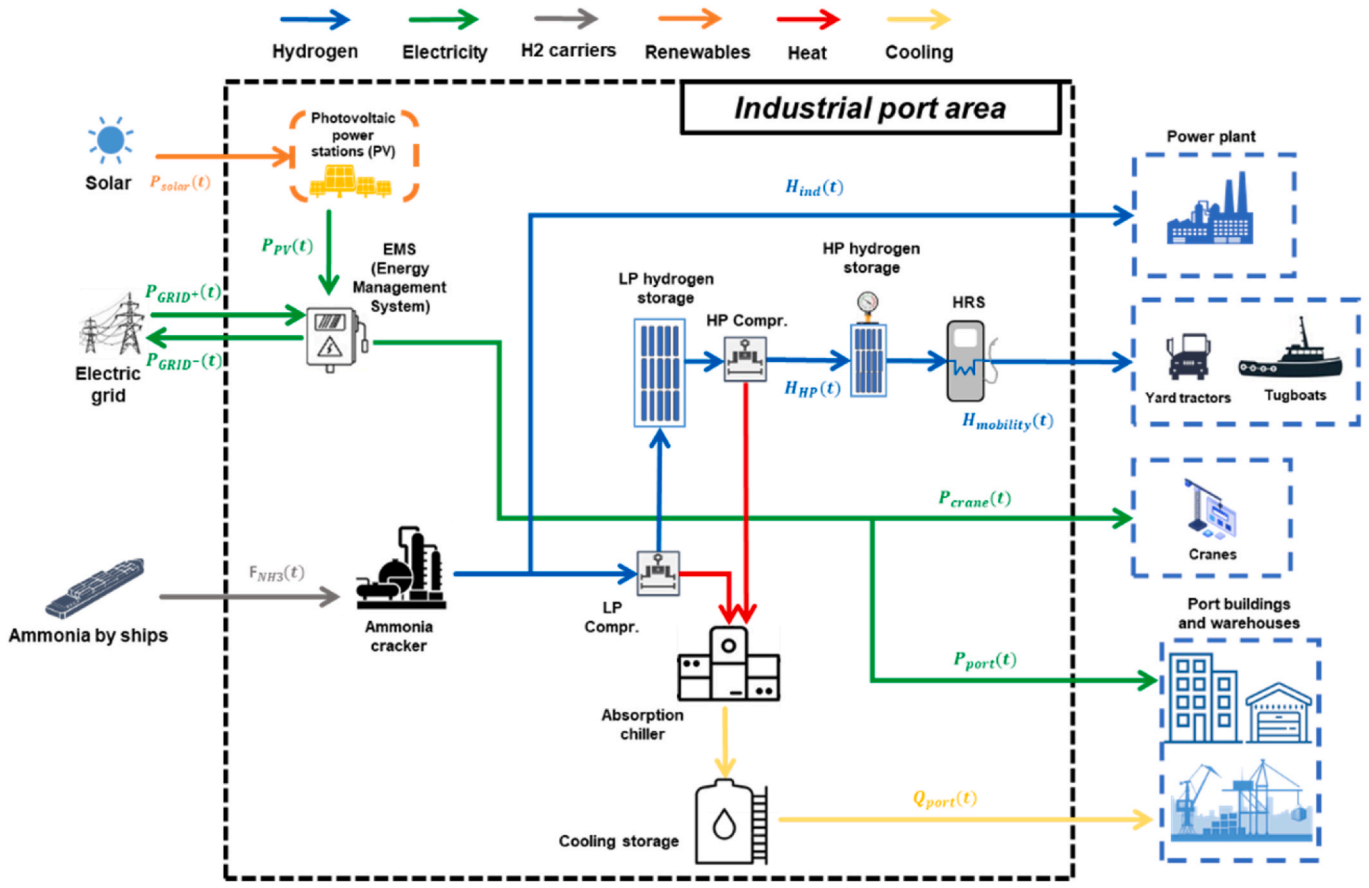

Fig. 18. Simplified schematic of the Config. 4. Energy conversion and storage units optimally selected by the optimization tool are included in the energy system configuration.

the table, the higher demand of H_2 for the CCGT plant implies higher storage capacity of the H_2 carriers (mostly NH_3) by almost one order of magnitude compared to Config.3. Whereas the import of LOHC is considered only when its cost is 30 % lower than the CC, the import of LH_2 results economically convenient for a 30 % reduction of its cost or for a 30 % higher cost of NH_3. In these scenarios, imported LH_2 and its regasification fulfil the entire IPA H_2 and port cooling demands, respectively. In the other scenarios, cooling demand is covered by the cooling generated by the ABC powered by the waste heat recovered from the compressors.

4.5. Gobal configurations comparison and final remarks

Considering the current energy and market scenario (CC), the total costs and emissions evaluated from optimizations for the four sub-structures are plotted in Figs. 23 and 24, respectively. In particular,

Table 4
Optimal design of energy conversion and storage units of configuration 4 in the differen energy and market scenarios.

	CC	−30 % CAPEX AEL	−50 % CAPEX AEL	−30 % CAPEX FC	−50 % CAPEX FC	+30 % cost LH_2	−30 % cost LH_2	+30 % cost LOHC	−30 % cost LOHC	+30 % cost NH_3	−30 % cost NH_3	Carbon tax 32 €/t	Carbon tax 56 €/t	Inflat. rate 3 %	Inflat. rate 8 %	Inflat. rate 12 %
PV (MWp)	**10.2**	**10.2**	**10.2**	**10.2**	**10.2**	**10.7**	**10.1**	**10.2**	**30.0**	**9.4**	**10.2**	**10.2**	**10.7**	**12.3**	**11.6**	**9.1**
Alkaline electrolyzer (kW)	0	0	0	0	0	0	0	0	0	0	0	0	0	0	0	0
FC (kW)	0	0	0	0	0	0	0	0	0	0	0	0	0	0	0	0
LP compressor (kW)	**731.8**	**730.8**	**731.8**	**731.8**	**731.8**	**753.1**	**549.8**	**731.8**	**443.5**	**443.5**	**731.8**	**740.2**	**746.4**	**800.5**	**800.5**	**584.1**
HP compressor (kW)	**275.4**	**275.4**	**275.4**	**275.4**	**275.4**	**275.4**	**275.4**	**275.4**	**275.4**	**275.4**	**275.4**	**275.4**	**275.4**	**275.4**	**275.4**	**275.4**
H_{LP} storage (kg)	**1142.0**	**1151.3**	**1142.8**	**1142.0**	**1142.0**	**987.3**	**2466.1**	**1142.8**	**3163.7**	**3237.3**	**1142.8**	**1055.7**	**1034.8**	**258.9**	**375.2**	**2216.7**
H_{HP} storage (kg)	**573.9**	**571.9**	**573.3**	**573.9**	**573.9**	**574.0**	**571.4**	**573.3**	**571.4**	**571.4**	**573.3**	**599.2**	**574.9**	**958.3**	**841.9**	**571.4**
Refrigerator for HRS (kW)	**176.8**	**176.8**	**176.8**	**176.8**	**176.8**	**176.8**	**176.8**	**176.8**	**176.8**	**176.8**	**176.8**	**176.8**	**176.8**	**176.8**	**176.8**	**176.8**
Grid capacity (MW)	**2.7**	**2.7**	**2.7**	**2.7**	**2.7**	**2.7**	**2.7**	**2.7**	**14.6**	**2.7**	**2.7**	**2.7**	**2.7**	**2.5**	**2.6**	**2.7**
Vapour compr. chiller (kW)	0	0	0	0	0	**14.2**	0	0	0	0	0	0	**11.4**	**11.1**	0	**28.4**
Absorption chiller (kW)	**927.0**	**925.8**	**927.0**	**927.0**	**927.0**	**935.7**	0	**927.0**	**760.5**	0	**927.0**	**933.5**	**933.5**	**1025.7**	**1020.5**	**764.4**
Cooling energy storage (MWh)	**3.8**	**3.8**	**3.8**	**3.8**	**3.8**	**4.3**	0	**3.8**	**1.4**	0	**3.8**	**3.9**	**4.1**	**5.7**	**5.7**	**3.7**
NH_3 cracker (MW)	**32.2**	**32.2**	**32.2**	**32.2**	**32.2**	**32.2**	0	**32.2**	0	0	**32.2**	**32.2**	**32.2**	**32.2**	**32.2**	**32.0**
NH_3 storage (t)	**5363.6**	**5363.6**	**5363.6**	**5363.6**	**5363.6**	**5363.6**	0	**5363.6**	0	0	**5363.6**	**5363.6**	**5363.6**	**5363.6**	**5363.6**	**5363.6**
LOHC dehydr. unit (t/h)	0	0	0	0	0	0	0	0	**33.3**	0	0	0	0	0	0	0
LOHC storage (t)	0	0	0	0	0	0	0	0	**5586.1**	0	0	0	0	0	0	0
LH_2 vaporizer (t/h)	0	0	0	0	0	0	**27.0**	0	0	**27.0**	0	0	0	0	0	0
LH_2 storage (t)	0	0	0	0	0	0	**4529.3**	0	0	**4529.3**	0	0	0	0	0	0
Batt. Capacity (kWh)	0	0	0	0	0	0	0	0	0	0	0	0	0	0	0	0

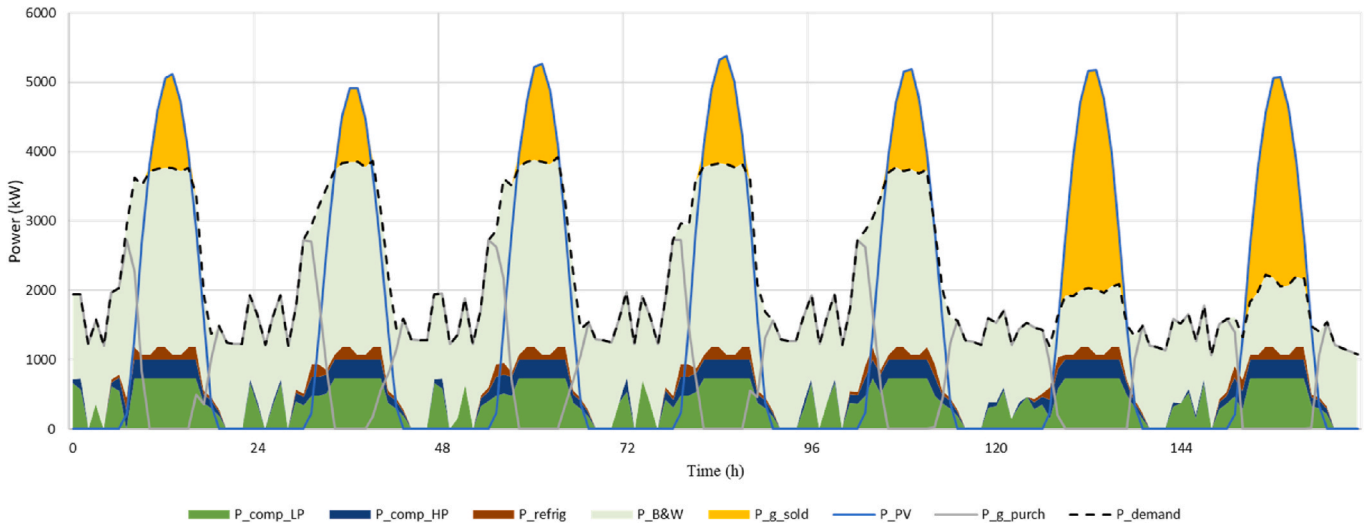

Fig. 19. Electric energy flows in the optimal operation of the energy system in the configuration 4.

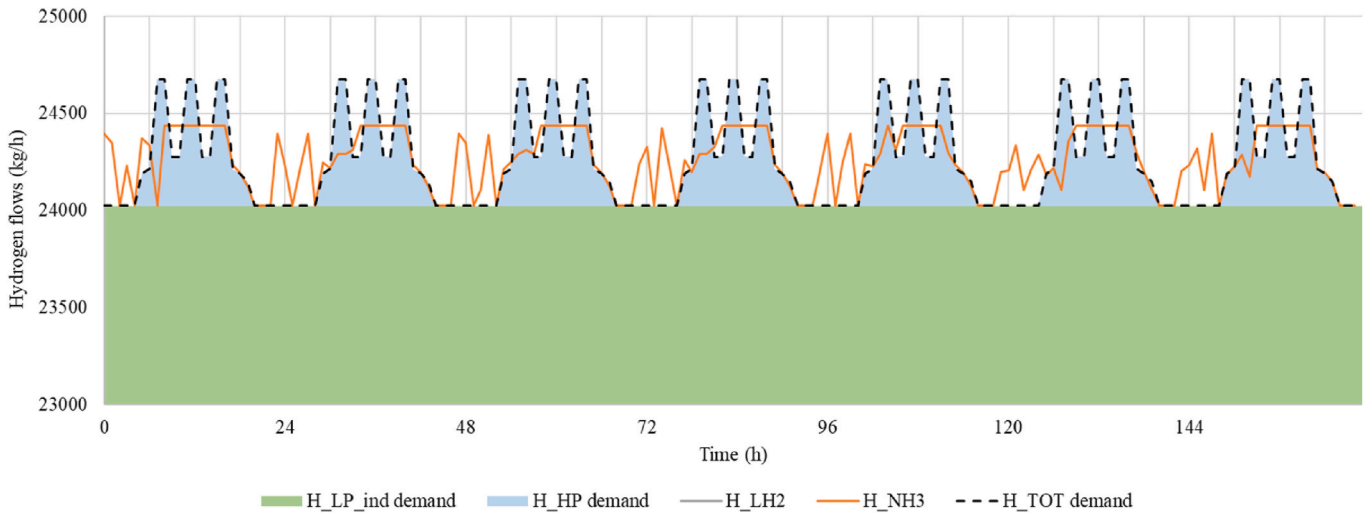

Fig. 20. H_2 flows in the optimal operation of the energy system in the configuration 4.

Fig. 23-A and Fig. 24-A focus on the costs and emissions related to the port energy system users, i.e. port vehicles, warehouses, and buildings, whereas Fig. 23-B and Fig. 24-B include also the costs and emissions related to the operation of CCGT power plant.

From the analysis of the results summarized in the various figures, it can be deduced that the CCGT power plant is responsible for ~97 % of the total carbon emissions generated by the IPA baseline configuration, which is attributed to the combustion of over 500 thousand tons of NG per year. The port operation energy related activities, which includes diesel-powered yard tractors and tugboats, as well as the energy supply to cranes, buildings, and warehouses, accounts for the remaining 3 % of emissions. Regarding the global share of the total costs, the purchase of NG for the CCGT plant accounts for more than 70 % of total costs in Configs. 0, 1 and 2, whereas, due to the significantly higher demand of H_2 imposed by the CCGT plant, the cost due to NG is limited only to 35 % in the Config. 3. Other main costs components are mostly related to the application of the carbon tax (up to 16 % share) and the NH_3 purchase with a 7 % and 53 % share in Configs. 3 and 4, respectively.

Blending H_2 with NG for supplying the CCGT plant can result in a significant reduction of carbon emissions. Fig. 24-B shows a notable 7 % and 50 % reduction of carbon emissions for Config. 3 (30%vol H_2) and Config. 4 (100%vol H_2), respectively. However, as expected, the greener configurations imply higher costs of up to 737 % compared to the baseline configuration since cost and carbon emissions are often conflicting objectives. Due to the high share of CCGT emissions compared to other sources, Config. 1 and Config. 2 do not lead to a reduction in emissions when both the power plant and port users are considered. However, as shown in Fig. 24-A, if the analysis is limited to the port area only, the implementation of new energy technologies can reduce total emissions by approximately 30 % and lower the total cost by around 20 % compared to the baseline case (Config. 0). Additionally, the installation of hybrid H_2-powered tugboats and yard tractors (Config. 2) results in a higher reduction of carbon emissions (66 %). However, from a cost perspective, Config. 2 is 35 % more expensive than Config. 0 due to the higher operational cost of the newly introduced energy carrier (H_2).

Comparing the optimal design of energy units presented in Table 1-Table 4, the LIB and the HT-PEMFC are not convenient to be installed and operated in the considered IPA.

A similar result emerges in Ref. [55] where LIB were not chosen as the optimal solution for storing electricity in the port. For HT-PEMFC, on the other hand, high costs limit their installation today, as emerges in Ref. [52]. Considering the current energy and market scenario (CC), nor are electrolysers and technologies for importing LOHC an economically feasible solution in the various substructures of the energy system.

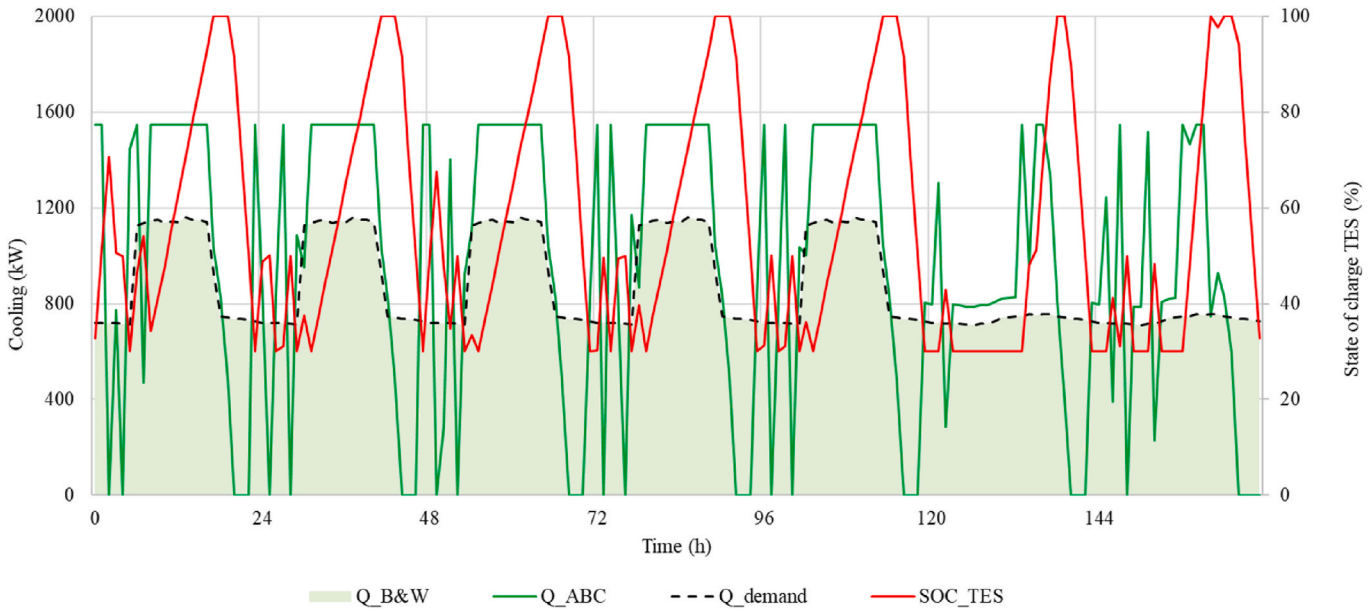

Fig. 21. Cooling energy flows in the optimal operation of the energy system in the configuration 4.

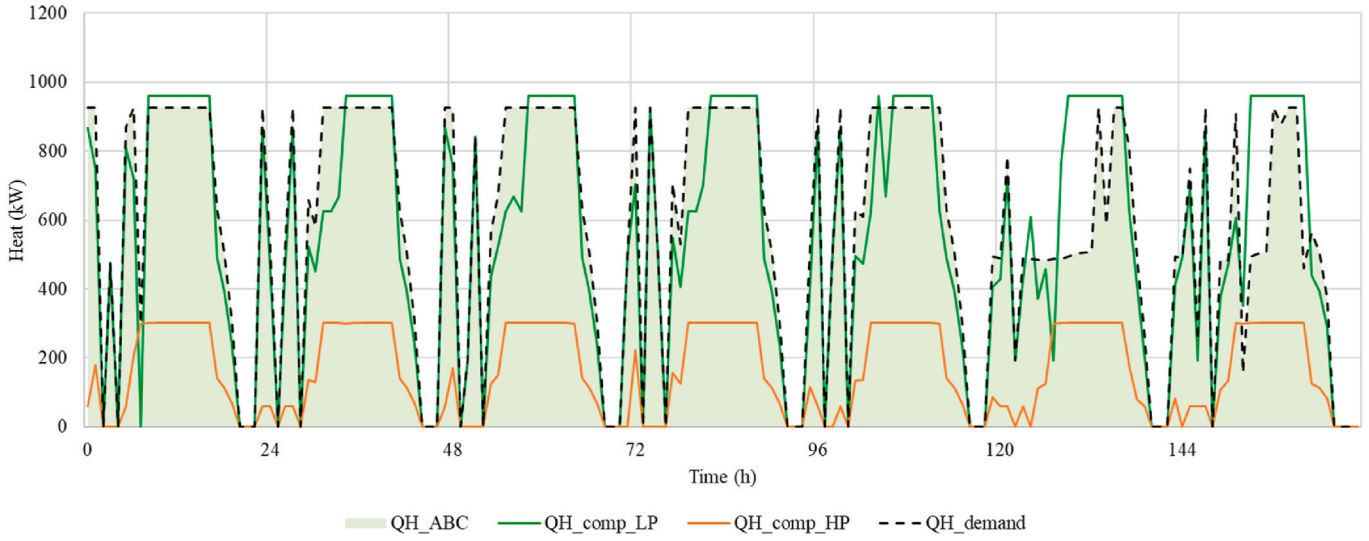

Fig. 22. Heating energy flows in the optimal operation of the energy system in the configuration 4.

To store the H_2 carriers when they are delivered by the ships in the port, the IPA utilizes large NH_3 and LH_2 storage systems. As also emerged in previous work of the authors [34,73], compressed H_2 storage systems are also installed to act as buffers between the LP and HP compressors and to store H_2 for use by yard tractors and tugboats, helping to limit the compressor power installed.

NH_3 results to be the most economically convenient H_2 carrier both for mobility and industrial supply. Nevertheless, LH_2 could be a promising alternative solution only with a substantial cost reduction. In addition, another great advantage of LH_2 is related to its high exergetic cryogenic value. Indeed, as shown in Config. 3 and Config. 4, when a −30 % LH_2 cost is reduced or when a +30 % NH_3 cost is increased the main other advantage of LH_2 is due to the potential to recover the waste cold from the regasification process to directly meet the cooling demand of port buildings and warehouses, thus avoiding the costs associated with the installation of VCC and/or ABC. However, ABC proves also to be a cost-effective solution for cold generation for buildings and warehouses due to the availability of the waste heat from H_2 compression.

The local production of H_2 with an AEL could supply a small amount of the H_2 required by IPA. For instance, in Config. 3, when NH_3 and LH_2 have a +30 % higher cost, the installation of the AEL results economically convenient. LOHC is a cost-effective solution to import H_2 only considering a 30 % lower cost of LOHC respect to the CC scenario.

Comparatively assessing the optimizations results subject to a carbon tax ranging from 18 to 56 €/tCO2,eq, it can be firstly concluded that the carbon tax has a negligible impact on the optimal design and operation of the energy systems, resulting in a minimal variation of total emissions (less than 2 %).

5. Conclusions

The study proposes a methodology to quantitatively assess the impact in term of cost and carbon emissions of different energy solutions and decarbonization strategies for IPAs. A multi-objective planning tool has been developed, tested, and validated against available dataset for enhanced robustness. The tool has been adopted to perform

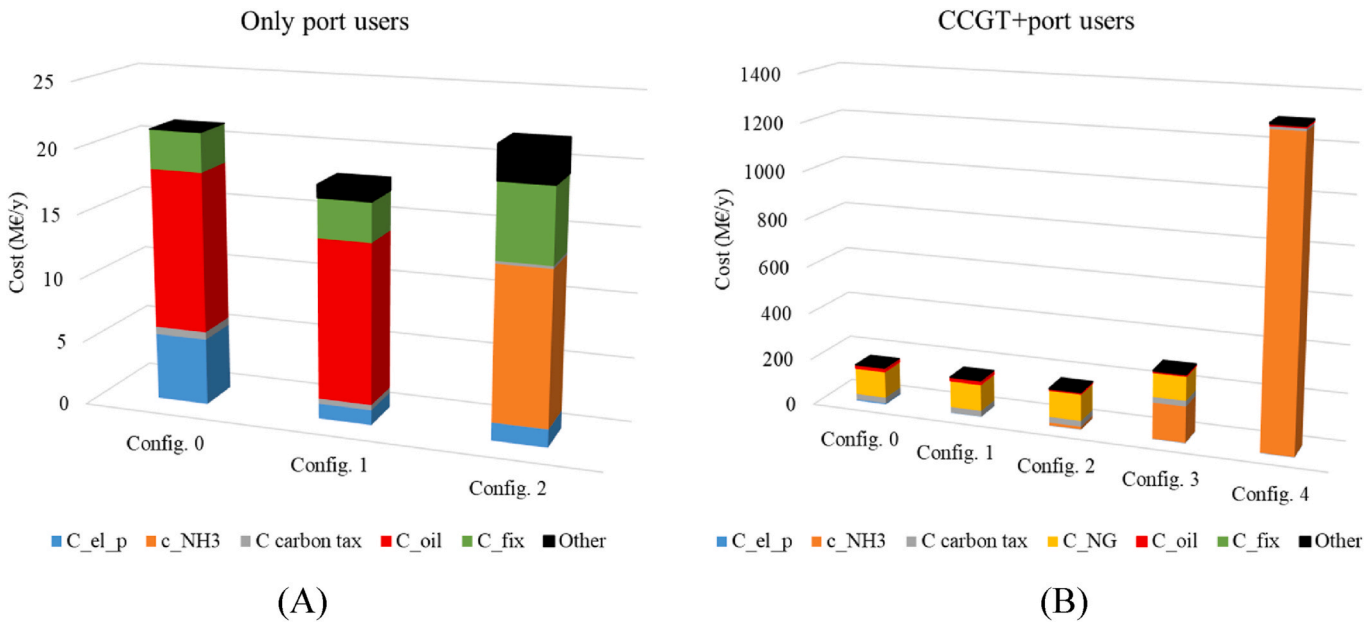

Fig. 23. Costs of the different energy system configurations proposed for the IPA. Blue bars identify the cost related to the purchase of electricity from the grid, orange bars the cost of NH_3 imported via ship, grey bars the cost associated with the emission of $CO_{2,eq}$ (carbon tax), yellow bars the cost of natural gas used by the CCGT plant, red bars the cost of Diesel oil used by port yard tractors and thugboats, grey bars the depreciation costs for vehicles and new infrastructures, black bars the other costs. A) refers to the costs of only the port energy users, B) refers to the costs of the CCGT power plant and the port energy users.

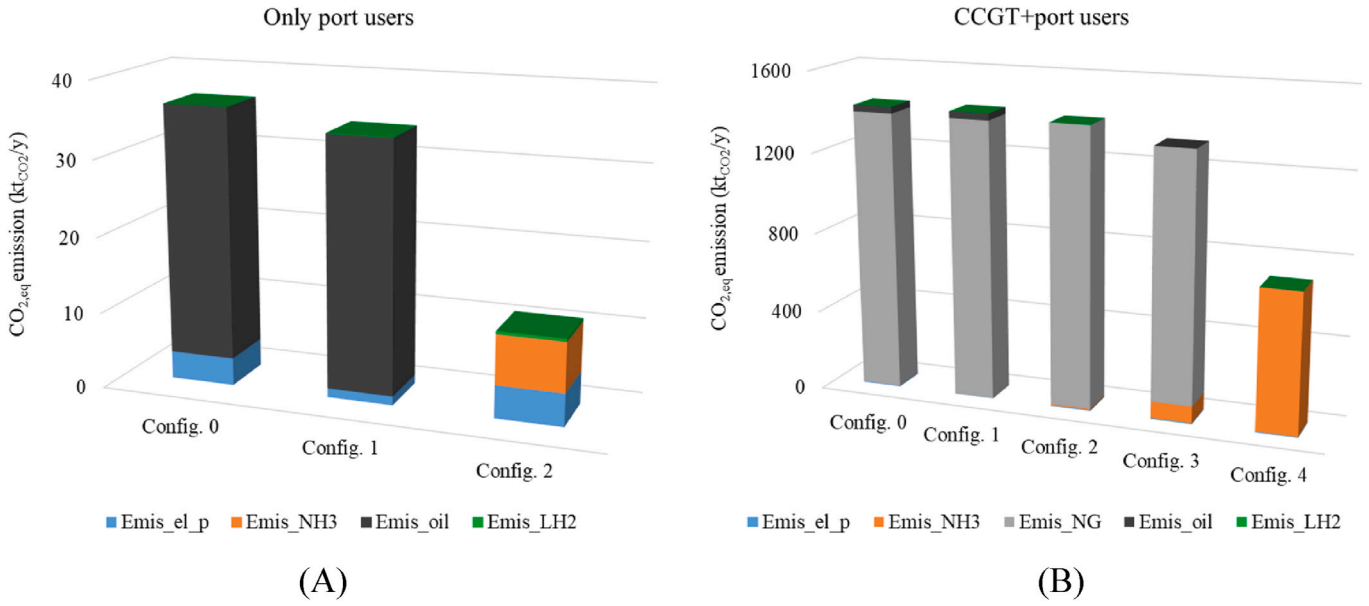

Fig. 24. $CO_{2,eq}$ emissions related to the yearly operation of the different energy system configurations proposed for the IPA. Blue bars identify the emissions related to the purchase of electricity from the grid, orange bars the emissions related to the import of NH_3 via ship, grey bars the emissions related to the combustion of natural gas in the CCGT plant, black bars the emissions related to the combustion of Diesel oil in port yard tractors and thugboats engines, green bars the emissions related to the import of LH_2 via ship. A) refers to the $CO_{2,eq}$ emissions of only the port energy users, B) refers to the $CO_{2,eq}$ emissions of the CCGT power plant and the port energy users.

optimization addressed to find optimal design and operation of energy units chosen to decarbonize a novel H_2-based port green energy hub. The developed tool is applied to the case study of an IPA located in tropical area. A typical operation week is taken as reference for the whole operation year of the system due to the characteristic climate region and latitude. Energy demand is analysed and synthetized and a set of decarbonization strategies is proposed to decarbonize the IPA operation. In particular, strategies include the exploitation of available solar energy, the production and import of H_2, the use of H_2 as fuel for port vehicles and equipment, and the H_2 use as primary energy source for the progressive decarbonization of a CCGT power plant.

The operation of the CCGT power plant has a significant impact on the carbon emissions in the port area, accounting for 97.5 % of the total carbon emissions. In addition, the CCGT plant operation accounts for more than 70 % of the total IPA cost due to the significant amount of natural gas and/or H_2 purchased.

The optimization results demonstrate that H_2 technologies can have a great impact on the reduction of carbon emissions in the IPA. In

particular, the replacement of Diesel engines with hybrid FC powertrains in tugboats and yard tractors can notably enhance the energy efficiency and reduce carbon emissions, potentially reaching outstanding zero emissions operation. In fact, these vehicles, often use by ports and hard to be electrified, are characterised by frequent work shifts and a high energy demand. However, electrification can be adopted for other port vehicles and equipment where direct connection to the grid is potentially applicable, such as electric cranes. As for the industrial sectors, it is demonstrated that industries located near ports can benefit from the easy access to H_2 from ports to decarbonize their operations. The replacement of fossil-based energy carriers with H_2 can have a great impact on the emissions reduction in the IPA. In particular, if the CCGT is fuelled with 100 % H_2 as in Config. 4, a 50 % reduction in emissions could be achieved. It is important to note that this configuration incurs a significant increase in total cost, more than seven times higher than the baseline configuration. If the CCGT plant is powered with a 30 % blend of H_2, as in Config. 3, only a 7 % reduction of emissions can be achieved. Considering only the energy demand of the port, the implementation of new energy conversion and storage units proposed in Config. 1 and 2 could have a significant impact on $CO_{2,eq}$ emissions, resulting in a 30 % and 66 % reduction compared to the baseline configuration, respectively. Moreover, Config. 1 leads to a 20 % costs reduction compared to the baseline, making it an economically and environmentally effective strategy for port decarbonization. The current carbon tax and the higher carbon taxes expected over the next two decades, whose values range from 18 to 56 €/$t_{CO2,eq}$, do not affect the optimal design of energy system components, although there are slight variations in the operation and total emissions of the energy system (about 2 % of the total value). The carbon tax approach appears to be ineffective in promoting carbon emission reductions for IPAs. In fact, carbon taxes are not sufficiently high to encourage the installation of new technologies with a lower environmental impact than conventional ones, which are still preferred despite higher operating costs.

The local production of H_2 via electrolysis results to be a cost-effective strategy only when the capital cost of AEL is reduced at least by 30 % compared to the current value. In this case, H_2 can also help in reducing the mismatch between RES production and electricity demand. The import of green H_2 carriers plays another key important role for the IPA decarbonization process. In particular, the optimization results show that NH_3 is the most economically convenient H_2 carrier. In fact, prevision of costs for green NH_3 are promising compared to the costs of the other H_2 carriers (i.e. LH_2 and LOHC), mainly due to the well-established and already existing NH_3 supply chain. Indeed, conversion technologies involving H_2 to NH_3 (Haber-Bosch process) and NH_3 to pure H_2 (NH_3 cracking process) are also already available at industrial large scale. Differently, LOHC technologies are less widespread, mature and available on a large scale. LH_2 import via ship might be also a promising option that can be effectively used in the next decades if the cost of liquefaction plant will be reduced, in parallel with an enhancement of the liquefaction performance. At the moment, the LH_2 widespread use is limited by the reduced capacity of liquefaction plants worldwide and by the high cost related to LH_2 production and distribution.

When choosing the best technologies for ports, incentive measures for H_2 technologies and/or the production and sale of green H_2 could have a considerable impact on the development and scale-up of these technologies. Furthermore, incentives on the use of these technologies could promote a more effective decarbonization of complex industrial areas, without substantially affecting the economic sustainability of the processes. Other form of financial support should be evaluated to ensure the economic competitiveness of H_2 technologies, such as electrolyzers and stationary FC. In addition, life cycle assessment could be performed to evaluate the cradle-to-crave carbon impact of such technologies. Lastly, the difficulty in making reliable predictions about all input parameters may change these results, as demonstrated by the results of sensitivity analysis performed for some of the model input parameters. Future developments could consider a wider range of their values and/or the analysis of other model parameters.

CRediT authorship contribution statement

Davide Pivetta: Writing – review & editing, Writing – original draft, Software, Methodology, Conceptualization. **Alessio Tafone:** Writing – review & editing, Writing – original draft, Validation, Methodology, Conceptualization. **Stefano Mazzoni:** Writing – review & editing, Methodology, Conceptualization. **Alessandro Romagnoli:** Supervision, Conceptualization. **Rodolfo Taccani:** Writing – review & editing, Supervision, Methodology, Conceptualization.

Declaration of competing interest

The authors declare that they have no known competing financial interests or personal relationships that could have appeared to influence the work reported in this paper.

Acknowledgements

D.P. and R.T. acknowledge the financial support from the project sHYpS (sustainable HYdrogen powered Shipping, Horizon Europe call Horizon-CL5-2021-D5-01).

Appendix A. Supplementary data

Supplementary data to this article can be found online at https://doi.org/10.1016/j.renene.2024.120979.

References

[1] UNCTAD, Review of Maritime Transport, 2022.
[2] United Nations Conference on Trade and Development (UNCTAD), Review of Maritime Transport, 2022. https://unctad.org/rmt2022. (Accessed 2 March 2023).
[3] K.L. Rødseth, H. Schøyen, P.B. Wangsness, Decomposing growth in Norwegian seaport container throughput and associated air pollution, Transp. Res. Part D Transp. Environ. 85 (2020) 102391, https://doi.org/10.1016/j.trd.2020.102391.
[4] J.-P. Rodrigue, Chapter 8.3 – ports and energy, in: Port Econ. Manag. Policy, n.d. 10.4324/9780429318184.
[5] G.L. Dnv, Ports: Green Gateways to Europe, 2022. https://www.dnv.com/Publications/ports-green-gateways-to-europe-179372. (Accessed 1 March 2023).
[6] M. Casazza, M. Lega, E. Jannelli, M. Minutillo, D. Jaffe, V. Severino, S. Ulgiati, 3D monitoring and modelling of air quality for sustainable urban port planning: review and perspectives, J. Clean. Prod. 231 (2019) 1342–1352, https://doi.org/10.1016/j.jclepro.2019.05.257.
[7] Y. Zheng, J. Zhao, G. Shao, Port city sustainability: a review of its research trends, Sustain. Times 12 (2020) 1–17, https://doi.org/10.3390/su12208355.
[8] Sustainable blue economy, (n.d.). https://oceans-and-fisheries.ec.europa.eu/ocean/blue-economy/sustainable-blue-economy_it (accessed October 10, 2023).
[9] Green airports and ports as multimodal hubs for sustainable and smart mobility | The European Maritime Spatial Planning Platform, (n.d.). https://maritime-spatial-planning.ec.europa.eu/fundings/green-airports-and-ports-multimodal-hubs-sustainable-and-smart-mobility (accessed October 10, 2023).
[10] T. Gerres, J.P. Chaves Ávila, P.L. Llamas, T.G. San Román, A review of cross-sector decarbonisation potentials in the European energy intensive industry, J. Clean. Prod. 210 (2019) 585–601, https://doi.org/10.1016/J.JCLEPRO.2018.11.036.
[11] Ç. Iris, J.S.L. Lam, A review of energy efficiency in ports: operational strategies, technologies and energy management systems, Renew. Sustain. Energy Rev. 112 (2019) 170–182, https://doi.org/10.1016/J.RSER.2019.04.069.
[12] N. Sifakis, T. Tsoutsos, Planning zero-emissions ports through the nearly zero energy port concept, J. Clean. Prod. 286 (2021), https://doi.org/10.1016/j.jclepro.2020.125448.
[13] T.P.V. Zis, Prospects of cold ironing as an emissions reduction option, Transp. Res. Part A Policy Pract. 119 (2019) 82–95, https://doi.org/10.1016/J.TRA.2018.11.003.
[14] L. Zhang, Q. Zeng, L. Wang, How to achieve comprehensive carbon emission reduction in ports? A systematic review, J. Mar. Sci. Eng. 12 (2024) 715, https://doi.org/10.3390/JMSE12050715.
[15] K. Karagkouni, M. Boile, C. Orive, K. Karagkouni, M. Boile, Classification of green practices implemented in ports: the application of green technologies, tools, and strategies, J. Mar. Sci. Eng. 12 (2024) 571, https://doi.org/10.3390/JMSE12040571.
[16] M. Acciaro, H. Ghiara, M.I. Cusano, Energy management in seaports: a new role for port authorities, Energy Pol. 71 (2014) 4–12, https://doi.org/10.1016/J.ENPOL.2014.04.013.

[17] N.B. Ahamad, M. Othman, J.C. Vasquez, J.M. Guerrero, C.L. Su, Optimal sizing and performance evaluation of a renewable energy based microgrid in future seaports, in: Proc. IEEE Int. Conf. Ind. Technol., Institute of Electrical and Electronics Engineers Inc., 2018, pp. 1043–1048, https://doi.org/10.1109/ICIT.2018.8352322.

[18] D. Pivetta, C. Dall'Armi, P. Sandrin, M. Bogar, R. Taccani, The role of hydrogen as enabler of industrial port area decarbonization, Renew. Sustain. Energy Rev. 189 (2024), https://doi.org/10.1016/j.rser.2023.113912.

[19] G. Di Ilio, P. Di Giorgio, L. Tribioli, G. Bella, E. Jannelli, Preliminary design of a fuel cell/battery hybrid powertrain for a heavy-duty yard truck for port logistics, Energy Convers. Manag. 243 (2021) 114423, https://doi.org/10.1016/J.ENCONMAN.2021.114423.

[20] L. van Biert, M. Godjevac, K. Visser, P.V. Aravind, A review of fuel cell systems for maritime applications, J. Power Sources 327 (2016) 345–364, https://doi.org/10.1016/J.JPOWSOUR.2016.07.007.

[21] C. Dall'Armi, D. Pivetta, R. Taccani, Hybrid PEM fuel cell power plants fuelled by hydrogen for improving sustainability in shipping: state of the art and review on active projects, Energies 16 (2023) 2022, https://doi.org/10.3390/EN16042022/S1.

[22] M. Mac Kinnon, G. Razeghi, S. Samuelsen, The role of fuel cells in port microgrids to support sustainable goods movement, Renew. Sustain. Energy Rev. 147 (2021), https://doi.org/10.1016/j.rser.2021.111226.

[23] H-vision project, (n.d.). https://www.h-vision.nl/en (accessed March 13, 2023).

[24] IRENA (International Renewable Energy Agency), Global Hydrogen Trade to Meet the 1.5°C Climate Goal: Technology Review of Hydrogen Carriers, Glob. Hydrog. Trade to meet 1.5°C clim, Goal Technol. Rev. Hydrog. Carriers, 2022. https://www.irena.org/publications/2022/Apr/Global-hydrogen-trade-Part-II. (Accessed 13 March 2023).

[25] H2PORTS Project, (n.d.). https://h2ports.eu/(accessed March 13, 2023).

[26] H2Valleys, Mission Innovation Hydrogen Valley Platform, (n.d.). https://h2v.eu/(accessed July 26, 2022).

[27] G. Mallouppas, C. Ioannou, E.A. Yfantis, A review of the latest trends in the use of green ammonia as an energy carrier in maritime industry, Energies 15 (2022) 1453, https://doi.org/10.3390/EN15041453.

[28] Maritime & Port Authority of Singapore (MPA), Maritime Singapore Decarbonisation Blueprint, n.d. https://www.mpa.gov.sg/maritime-singapore/sustainability/maritime-singapore-decarbonisation-blueprint (accessed March 6, 2023).

[29] Energy Market Authority (EMA), Charting the Energy Transition to 2050 - Energy 2050 Committee Report, 2022.

[30] Maritime Singapore Green Initiative | Maritime & Port Authority of Singapore (MPA), (n.d.).

[31] A.S. Alamoush, F. Ballini, A.I. Ölçer, Ports' technical and operational measures to reduce greenhouse gas emission and improve energy efficiency: a review, Mar. Pollut. Bull. 160 (2020), https://doi.org/10.1016/j.marpolbul.2020.111508.

[32] Open Energy Modelling Framework (oemof) — oemof documentation, (n.d.). https://oemof.readthedocs.io/en/latest/(accessed October 10, 2023).

[33] Digitalizing real estate for sustainability | OPTIML, (n.d.). https://www.optiml.com/(accessed October 10, 2023).

[34] D. Pivetta, G. Volpato, G. Carraro, C. Dall'Armi, L. Da Lio, A. Lazzaretto, R. Taccani, Optimal decarbonization strategies for an industrial port area by using hydrogen as energy carrier, Int. J. Hydrogen Energy 52 (2024) 1084–1103, https://doi.org/10.1016/J.IJHYDENE.2023.07.008.

[35] U. Klanšek, A comparison between MILP and MINLP approaches to optimal solution of Nonlinear Discrete Transportation Problem, Vilnius Gedim. Tech. Univ. 30 (2015) 135–144, https://doi.org/10.3846/16484142.2014.933361.

[36] S. Rech, Smart energy systems: guidelines for modelling and optimizing a fleet of units of different configurations, Energies 12 (2019) 1320, https://doi.org/10.3390/EN12071320.

[37] S. Consonni, G. Lozza, E. Macchi, Optimization of cogeneration systems operation—Part B: solution algorithm and examples of optimum operating strategies, in: ASME Int. Symp. Turbomachinery, Comb. Technol. Cogener., Nice, France, 1989.

[38] K. Ito, R. Yokoyama, S. Akagi, T. Yamaguchi, Y. Matsumoto, Optimal operational planning of a gas turbine combined heat and power plant based on the mixed-integer programming, IFAC Proc 21 (1988) 371–377, https://doi.org/10.1016/S1474-6670(17)53769-6.

[39] S. Rech, Analisi e ottimizzazione della configurazione di un macrosistema di conversione di energia, Università degli studi di Padova, 2013, 10.2/JQUERY.MIN.JS.

[40] D. Pivetta, C. Dall'Armi, R. Taccani, Multi-objective optimization of hybrid PEMFC/Li-ion battery propulsion systems for small and medium size ferries, Int. J. Hydrogen Energy 46 (2021) 35949–35960, https://doi.org/10.1016/J.IJHYDENE.2021.02.124.

[41] C. Dall'Armi, D. Pivetta, R. Taccani, Uncertainty analysis of the optimal health-conscious operation of a hybrid PEMFC coastal ferry, Int. J. Hydrogen Energy (2021), https://doi.org/10.1016/J.IJHYDENE.2021.10.271.

[42] P. Gabrielli, M. Gazzani, E. Martelli, M. Mazzotti, Optimal design of multi-energy systems with seasonal storage, Appl. Energy 219 (2018) 408–424, https://doi.org/10.1016/J.APENERGY.2017.07.142.

[43] Python.org Website, (n.d.).

[44] Gurobi Optimization Website, (n.d.).

[45] K. Ito, R. Yokoyama, T. Shiba, Optimal operation of a diesel engine cogeneration plant including a heat storage tank, J. Eng. Gas Turbines Power 114 (1992) 687–694, https://doi.org/10.1115/1.2906643.

[46] S. Rech, A. Lazzaretto, Smart rules and thermal, electric and hydro storages for the optimum operation of a renewable energy system, Energy 147 (2018) 742–756, https://doi.org/10.1016/J.ENERGY.2018.01.079.

[47] Renewables.ninja website, (n.d.). https://www.renewables.ninja/(accessed March 2, 2023).

[48] Energy Market Authority (EMA), Electricity market data, (n.d.). https://www.ema.gov.sg/resources/statistics (accessed September 29, 2023).

[49] Electricity Maps website, (n.d.). https://www.electricitymaps.com/(accessed March 2, 2023).

[50] De Nora, alkaline electrolyzer, (n.d.). https://www.denora.com/it/applications/H2-production-by-water-electrolysis.html (accessed May 24, 2024).

[51] X. Cao, J. Wang, P. Zhao, H. Xia, Y. Li, L. Sun, W. He, Hydrogen production system using alkaline water electrolysis adapting to fast fluctuating photovoltaic power, Energies 16 (2023) 3308, https://doi.org/10.3390/EN16083308.

[52] V. Cigolotti, M. Genovese, Stationary Fuel Cell Applications: Current and Future Technologies - Costs, Performances, and Potential, (n.d.).

[53] Hyjack website, (n.d.). https://hyjack.tech/(accessed March 2, 2023).

[54] S. Mazzoni, S. Ooi, B. Nastasi, A. Romagnoli, Energy storage technologies as techno-economic parameters for master-planning and optimal dispatch in smart multi energy systems, Appl. Energy 254 (2019) 113682, https://doi.org/10.1016/J.APENERGY.2019.113682.

[55] A. Tafone, S. Raj Thangavelu, S. Morita, A. Romagnoli, Design optimization of a novel cryo-polygeneration demonstrator developed in Singapore – Techno-economic feasibility study for a cooling dominated tropical climate, Appl. Energy 330 (2023) 119916, https://doi.org/10.1016/J.APENERGY.2022.119916.

[56] K.H. Chua, Y.S. Lim, S. Morris, Cost-benefit assessment of energy storage for utility and customers: a case study in Malaysia, Energy Convers. Manag. 106 (2015) 1071–1081, https://doi.org/10.1016/J.ENCONMAN.2015.10.041.

[57] J2601_201407: Fueling Protocols for Light Duty Gaseous Hydrogen Surface Vehicles - SAE International, (n.d.). https://www.sae.org/standards/content/j2601_201407/(accessed March 2, 2023).

[58] I.H. Bell, J. Wronski, S. Quoilin, V. Lemort, Pure and pseudo-pure fluid thermophysical property evaluation and the open-source thermophysical property library coolprop, Ind. Eng. Chem. Res. 53 (2014) 2498–2508, https://doi.org/10.1021/ie4033999.

[59] CoolProp website, (n.d.)http://www.coolprop.org/index.html (accessed September 4, 2023).

[60] A. Riaz, M.R. Sarker, M.H.M. Saad, R. Mohamed, Review on comparison of different energy storage technologies used in micro-energy harvesting, WSNs, low-cost microelectronic devices: challenges and recommendations, Sensors 21 (2021) 5041, https://doi.org/10.3390/S21155041.

[61] Z. Cesaro, M. Ives, R. Nayak-Luke, M. Mason, R. Bañares-Alcántara, Ammonia to power: forecasting the levelized cost of electricity from green ammonia in large-scale power plants, Appl. Energy 282 (2021) 116009, https://doi.org/10.1016/J.APENERGY.2020.116009.

[62] F. Schreiner, M. Riemer, Conversion of LNG Terminals for Liquid Hydrogen or Ammonia, 2022.

[63] M. Reuß, T. Grube, M. Robinius, P. Preuster, P. Wasserscheid, D. Stolten, Seasonal storage and alternative carriers: a flexible hydrogen supply chain model, Appl. Energy 200 (2017) 290–302, https://doi.org/10.1016/J.APENERGY.2017.05.050.

[64] M. Hurskainen, J. Ihonen, Techno-economic feasibility of road transport of hydrogen using liquid organic hydrogen carriers, Int. J. Hydrogen Energy 45 (2020) 32098–32112, https://doi.org/10.1016/J.IJHYDENE.2020.08.186.

[65] Gurobi Optimization website, (n.d.). https://www.gurobi.com/(accessed March 15, 2022).

[66] A. Bartolini, S. Mazzoni, G. Comodi, A. Romagnoli, Impact of carbon pricing on distributed energy systems planning, Appl. Energy 301 (2021) 117324, https://doi.org/10.1016/J.APENERGY.2021.117324.

[67] Maritime & Port Authority of Singapore (MPA), Maritime Singapore Decarbonisation Blueprint, (n.d.). https://www.mpa.gov.sg/maritime-singapore/sustainability/maritime-singapore-decarbonisation-blueprint (accessed March 6, 2023).

[68] G. Di Ilio, P. Di Giorgio, L. Tribioli, V. Cigolotti, G. Bella, E. Jannelli, Assessment of a hydrogen-fueled heavy-duty yard truck for roll-on and roll-off port operations, SAE Tech. Pap. (2021), https://doi.org/10.4271/2021-24-0109.

[69] Keppel Infrastructure, Keppel to develop Singapore's first hydrogen-ready power plant, with construction undertaken by Mitsubishi Power Asia Pacific and Jurong Engineering consortium, (n.d.). https://www.kepinfra.com/en/news-item.aspx?aid=16124&title=keppel-to-develop-singapores-first-hydrogen-ready-power-plant (accessed March 6, 2023).

[70] Energy Market Authority (EMA), Charting the Energy Transition to 2050 - Energy 2050 Committee Report, 2022. https://www.ema.gov.sg/content/dam/corporate/resources/energy-2050-committee-report/EMA-Energy-2050-Committee-Report.pdf.coredownload.pdf. (Accessed 10 September 2023).

[71] Ministry of Trade and Industry Singapore, Singapore's National Hydrogen Strategy, (n.d.). https://www.mti.gov.sg/Industries/Hydrogen (accessed September 4, 2023).

[72] National Climate Change Secretariat (NCCS) Singapore, Singapore's climate actions - Carbon Tax, (n.d.). https://www.nccs.gov.sg/singapores-climate-action/carbon-tax/(accessed March 2, 2023).

[73] D. Pivetta, C. Dall'Armi, R. Taccani, Multi-objective optimization of a hydrogen hub for the decarbonization of a port industrial area, J. Mar. Sci. Eng. 10 (2022) 231. https://doi.org/10.3390/jmse10020231.